



## Satellite tools to monitor and predict Hurricane Sandy (2012): Current and emerging products



Michael J. Folmer <sup>a,\*</sup>, Mark DeMaria <sup>b</sup>, Ralph Ferraro <sup>c</sup>, John Beven <sup>b</sup>, Michael Brennan <sup>b</sup>, Jaime Daniels <sup>c</sup>, Robert Kuligowski <sup>c</sup>, Huan Meng <sup>c</sup>, Scott Rudlosky <sup>c</sup>, Limin Zhao <sup>d</sup>, John Knaff <sup>e</sup>, Sheldon Kusselson <sup>d</sup>, Steven D. Miller <sup>f</sup>, Timothy J. Schmit <sup>g</sup>, Chris Velden <sup>h</sup>, Brad Zavodsky <sup>i</sup>

<sup>a</sup> University of Maryland/ESSIC/CICS, College Park, MD, United States

<sup>b</sup> NOAA/NWS/NCEP/NHC, Miami, FL, United States

<sup>c</sup> NOAA/NESDIS/STAR, College Park, MD, United States

<sup>d</sup> NOAA/NESDIS/OSPO, College Park, MD, United States

<sup>e</sup> NOAA/NESDIS/STAR, Fort Collins, CO, United States

<sup>f</sup> Colorado State University/CIRA, Fort Collins, CO, United States

<sup>g</sup> NOAA/NESDIS/STAR, Madison, WI, United States

<sup>h</sup> University of Wisconsin-Madison/CIMSS, Madison, WI, United States

<sup>i</sup> NASA/SPoRT, Huntsville, AL, United States

### ARTICLE INFO

#### Article history:

Received 6 February 2015

Received in revised form 2 June 2015

Accepted 3 June 2015

Available online 11 June 2015

#### Keywords:

Remote sensing

Passive microwave

Hurricane

GOES-R

JPSS

Sandy

### ABSTRACT

Hurricane Sandy – a tropical cyclone that transitioned into an extratropical cyclone near the time of landfall along the east coast of the United States – caused historic damage in many regions which rarely receive such a direct hit from a storm of this magnitude, including many of the large metropolitan areas along the U.S. eastern seaboard. Specifically, Sandy generated record low-pressure, a large wind field with corresponding storm surge and copious amounts of precipitation in some areas, including record snowfall in mountainous regions. Sandy presented several forecast challenges to the National Oceanic and Atmospheric Administration's (NOAA) National Weather Service (NWS). Satellites played an integral role in the analysis and forecast of Sandy's track and intensity. The NOAA National Hurricane Center, Ocean Prediction Center, and Weather Prediction Center all relied on information from satellites to make critical warning decisions using various satellite products that assist with diagnosing tropical cyclone intensity, surface winds over the ocean, and heavy precipitation. All of the skillful global forecast models used satellite data for initiation to better forecast the track and intensity of Sandy. As part of the Geostationary Operational Environmental Satellite – R-series (GOES-R) and Joint Polar Satellite System (JPSS) Proving Ground activities, new satellite products were available to forecasters at these national centers in experimental form to assist with observing this unique, high impact event. This paper will demonstrate how the current satellite products assisted NOAA forecasters during Sandy and introduce some new satellite products that could be used to analyze and predict future high impact weather systems.

© 2015 Elsevier B.V. All rights reserved.

### 1. Introduction

From a meteorological perspective, Hurricane Sandy (henceforth simply referred to as Sandy) was a “perfect storm”. The convergence of several synoptic features phased together along the U.S. Mid-Atlantic coastline to create record low-pressure, a huge wind field with corresponding storm surge, and copious amounts of precipitation in some areas, including record snowfall. Sandy caused over 250 deaths and upwards of \$70 billion in damage

and economic loss during its trek from the Caribbean northward to the mid-Atlantic and Northeastern United States (Blake et al., 2013).

Satellite data are utilized in three primary ways for tropical cyclone (TC) analysis and prediction. First, they are used for situational awareness. For example, water vapor imagery loops from geostationary satellites are often used subjectively to assess the flow in the cyclone environment. Second, quantitative satellite products are used for storm analysis, such as satellite-based cyclone position and intensity estimates and sea surface temperature analyses. Third, satellite data are assimilated into numerical forecast models. All three of these applications were heavily utilized in Sandy. For example, numerical weather forecasts were generally very good, with models such as the National Oceanic and Atmospheric Administration (NOAA) National Center for Environmental Prediction's (NCEP) Global Forecast System (GFS) and

\* Corresponding author at: NOAA Center for Weather and Climate Prediction (NCWCP), 5830 University Research Court, Rm. 4000, College Park, MD 20740.

E-mail addresses: [Michael.Folmer@noaa.gov](mailto:Michael.Folmer@noaa.gov) (M.J. Folmer), [Mark.DeMaria@noaa.gov](mailto:Mark.DeMaria@noaa.gov) (M. DeMaria), [Ralph.R.Ferraro@noaa.gov](mailto:Ralph.R.Ferraro@noaa.gov) (R. Ferraro).

the European Centre for Medium-Range Weather Forecasts' (ECMWF) global model forecasting Sandy's intensity and track several days in advance. Satellite products aided the National Hurricane Center (NHC) with monitoring TC position and intensity, and column water vapor and precipitation estimates helped in assessing the location, duration and trends of the heaviest precipitation, especially when Sandy was offshore and out of radar range. Other satellite products such as sea surface temperature, oceanic heat content, and ocean surface vector winds also provided vital information to the forecasters. This paper illustrates many of the products that were available during Sandy and introduces proxy products demonstrating capabilities of future satellite missions.

Section 2 summarizes the life cycle of Sandy, Section 3 describes how satellite data and products contributed to the operational analysis and forecasting of Sandy's track, intensity, structure and precipitation, and Section 4 presents some emerging satellite capabilities. A summary and conclusions are presented in Section 5.

## 2. The life cycle of Sandy

Sandy's evolution is described in detail in the NHC Tropical Cyclone Report for this cyclone (Blake et al., 2013). Fig. 1 shows the track and intensity of Hurricane Sandy. Sandy originated from a tropical wave that left the west coast of Africa on 11 October. By 1200 UTC on 22 October, a surface circulation and banding features became organized enough about 560 km south-southwest of Kingston, Jamaica to be classified by the NHC as a tropical depression.

The depression rapidly organized in the next 6 h and was classified as Tropical Storm Sandy around 1800 UTC on 22 October. Steady strengthening occurred over the next 42 h and Sandy became a  $36 \text{ m s}^{-1}$  (70-kt) hurricane at the 1200 UTC NHC advisory on 24 October just before its first landfall in eastern Jamaica. After crossing Jamaica, Sandy continued to strengthen up until a second landfall in eastern Cuba as a  $52 \text{ m s}^{-1}$  (100-kt), Category 3 hurricane at 0525 UTC on 25 October. Sandy maintained hurricane intensity through the central Bahamas, though it did weaken after traversing the rugged terrain in Eastern Cuba and encountering southwesterly shear associated with

an upper-level low to the southwest. Following this interaction, Sandy took on a hybrid-like structure from 26 October to 27 October as the storm encountered dry air and increased vertical wind shear, briefly losing its hurricane status in the process (0000 UTC 27 October to 1200 UTC 27 October). Early on 28 October 2012, the hurricane's outflow wrapped around the southwest quadrant and the effects of the upper-low diminished. This allowed Sandy to re-intensify over the warm Gulf Stream waters east of North Carolina.

Late on 28 October 2012, the final in a series of shortwaves dropped from the Upper Plains of the U.S. toward the Carolinas and started to cut off an upper-low from the jetstream just west of Sandy. This allowed the upper-level low to capture Sandy early on 29 October 2012, resulting in a west-northwest motion toward the Mid-Atlantic coastline. Sandy was considered a hurricane up until the 2100 UTC 29 October 2012 NHC advisory when the storm merged with the upper-level low and transitioned into an extratropical storm (re-classified as post tropical – a storm that was once tropical and has since acquired non-tropical characteristics), including a warm seclusion structure surrounded by much colder air. Sandy continued west and made its final landfall in southern New Jersey with winds along the coast at hurricane strength (70-kt) with stronger wind gusts experienced well north of the landfall point. After landfall, Sandy moved into south-central Pennsylvania and fully occluded on 30 October 2012, slowly spinning down before being picked up by an upstream shortwave trough around 1 November 2012.

## 3. Satellite contributions to the analysis and forecasting of Sandy

The NHC provides a number of text and graphical products for tropical cyclones in the Atlantic and north East Pacific tropical cyclone basins. Details are available from [www.nhc.noaa.gov](http://www.nhc.noaa.gov). The primary forecast parameters are the latitude and longitude of the TC center, and maximum sustained surface winds, which are provided out to 120 h. Storm structure is represented by the radii of 34, 50 and 64 kt winds in four quadrants relative to the storm center (NE, SE, SW and NW). The 34 and 50 kt wind radii are forecasted out to 72 h and the 64 kt radii out to 36 h. The cyclone type (tropical, subtropical, extra-

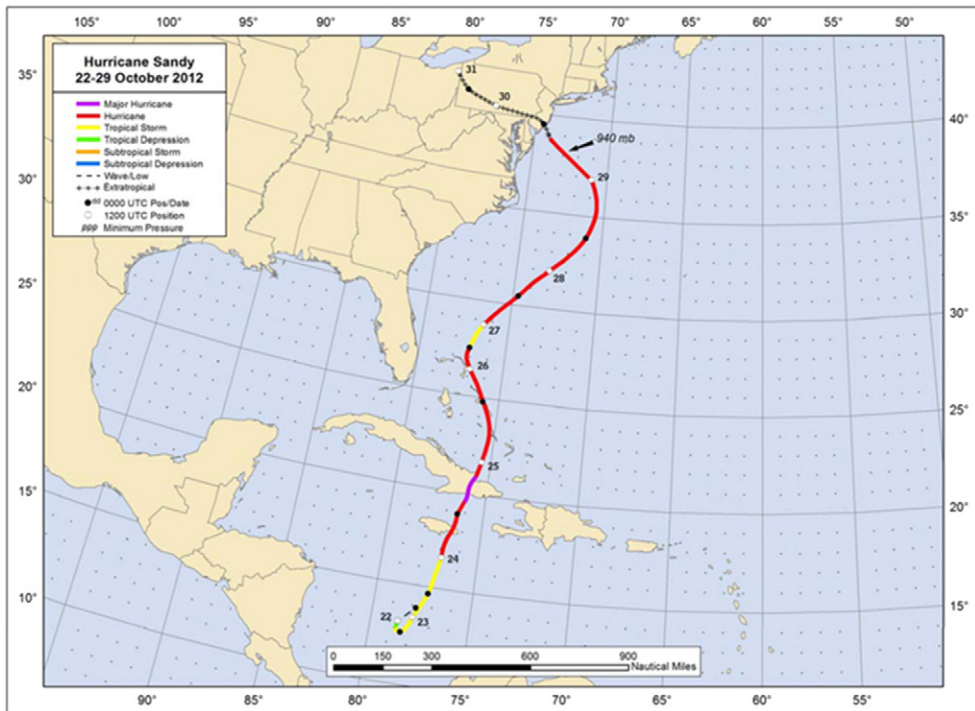


**Fig. 1.** The NHC best track and intensity of Hurricane Sandy.  
From Blake et al., 2013 [www.nhc.noaa.gov](http://www.nhc.noaa.gov).

tropical) is also estimated out to 120 h. NHC's forecasts are discontinued once a TC undergoes extra-tropical transition. NHC also estimates the probability of tropical cyclone formation from 0 to 48 h and from 0 to 120 h. All forecast parameters are updated every 6 h. NHC provides only general guidance on TC rainfall. The NCEP Weather Prediction Center (WPC) has the primary responsibility for quantitative precipitation estimates and forecasts for TCs. This section describes how satellite data and products were utilized to provide guidance to NHC and WPC for Hurricane Sandy.

### 3.1. Monitoring and real-time analysis

Tropical cyclones spend most of their lifetimes over tropical and subtropical oceans where conventional data are sparse, so utilization of satellite observations is crucial for accurate TC analyses and forecasts. Sandy was no exception. Advisory number 1, when Sandy first became a tropical depression, begins with "Satellite images and surface observations indicate that the low pressure system ... has sufficient organization to be classified as a tropical depression." Geostationary and low-earth orbiting (LEO) satellite data continued to be utilized in combination with aircraft and in situ data to monitor the structure of Sandy and its environment, and estimate the center position of the cyclone. Several satellite-based tools had great value for monitoring and analyzing Sandy and the near-storm environment, including the following:

#### 1) The Dvorak technique

Satellite data are fundamental to helping to determine the real-time intensity of TCs. The Dvorak technique, which estimates the maximum wind from visible and infrared imagery using pattern recognition techniques, has been the backbone of intensity estimation around the globe for several decades (Velden et al., 2006). While heavily used during Sandy, the unusual structure of the cyclone as it interacted with the nearby baroclinic features presented some challenges for the technique. The Dvorak technique worked reasonably well when the cyclone was south of the Bahamas and had a more typical tropical structure. However, in the last few days before landfall in the U.S., the maximum wind estimates were 10 to 15 kt too low because the convective organization was atypical and the cloud top temperatures were fairly warm. The minimum sea level

pressures had an extreme high bias (up to 60 hPa too high), partly because the maximum wind estimates were low, and partly because of the large size of the circulation. The pressure–wind relationship during this period was very different than that utilized by the Dvorak method.

#### 2) AMSU products

A key defining characteristic of a TC is a deep warm core structure. As a TC undergoes extratropical transition (ET), the warm core structure typically erodes from the lower-mid troposphere as cold air advection near the surface intrudes into the circulation. This evolution can often be depicted in cross-sections of thermal anomalies derived from Advanced Microwave Sounding Unit (AMSU) data. One such product used by the NHC to determine structure is derived in near real-time by the Cooperative Institute for Meteorological Satellite Studies (CIMSS) (Herndon and Velden, 2006) (<http://amsu.ssec.wisc.edu/>).

A good example of the utility of the AMSU data to depict this transitional phase occurred just prior to and after the landfall of Sandy. About 5 h before landfall in the U.S., the AMSU data showed a deep warm core (as evidenced by the brightness temperature anomalies in Fig. 2), particularly strong in the mid-levels, indicating that Sandy had not yet lost all of its TC characteristics. Then about 7 h after landfall, the warm core has eroded considerably (Fig. 3). By this time the NHC had declared Sandy post-tropical. AMSU data supported other aircraft-based observations in making the decision to declare Sandy extratropical.

The AMSU data are also used to provide operational intensity and wind structure estimates (Demuth et al., 2004, 2006; Herndon and Velden, 2006). One such method uses temperature retrievals as input to the hydrostatic equation to estimate the geopotential height field at the standard pressure levels from 100 to 1000 hPa. These fields provide input to statistical intensity and structure estimates. Additionally, the nonlinear balance equation is used to estimate the wind fields on standard pressure levels from the geopotential height field (Bessho et al., 2006). These routinely generated balanced winds are then used as input to the operational surface wind product described in Section 4. The horizontal resolution of the AMSU data is too coarse (50 km at nadir) to resolve the tight height gradients near the storm center, but the method provides reasonable wind estimates in the outer portions of the storm.

#### 3) Scatterometers

Forecasters at NHC and the Ocean Prediction Center (OPC) had access to

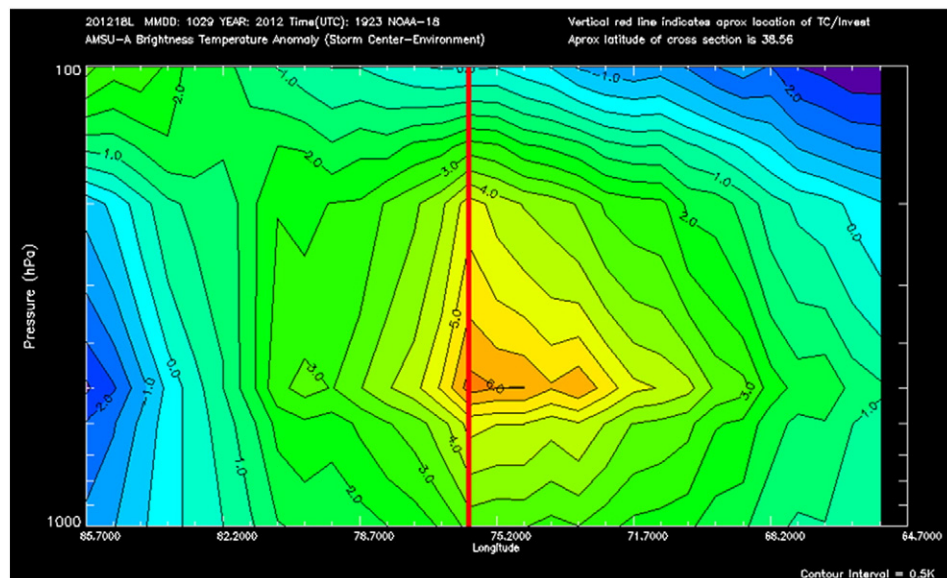


**Fig. 2.** Longitude-height cross sections of NOAA-18 AMSU-A brightness temperature anomaly at 1923 UTC on 29 October 2012 (4 h before landfall). The center of Sandy is indicated by the vertical red line.

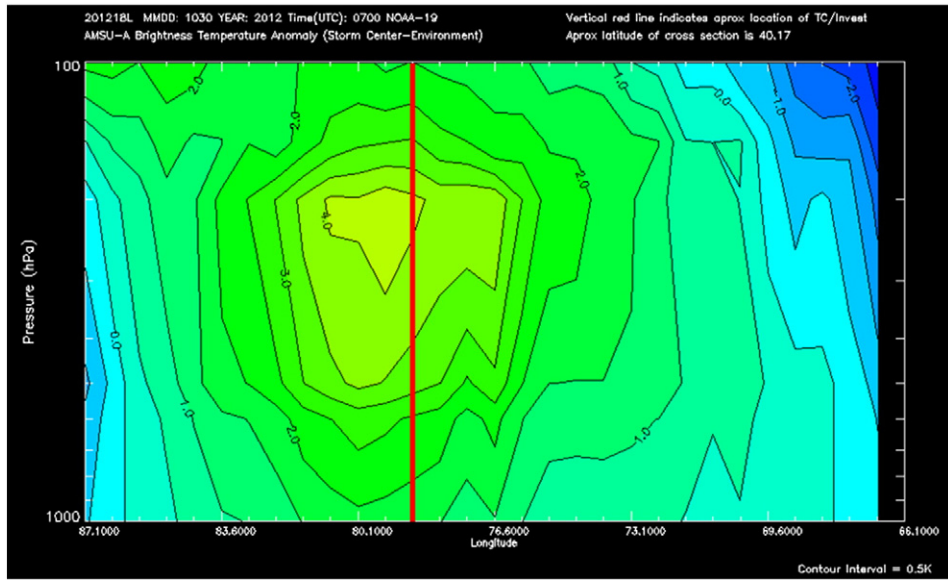


**Fig. 3.** Same as Fig. 2, but at 0700 UTC on 30 October 2012 (7.5 h after landfall) from NOAA-19.

ocean surface vector wind retrievals from the European Space Agency's Advanced Scatterometer (ASCAT) and the Indian Space Research Organization's Ocean Scatterometer (OSCAT) to monitor Sandy's wind structure. While rain and resolution issues hamper the use of scatterometer ocean surface vector wind data in the TC core, they can provide valuable information about the 34-kt wind field of TCs (Brennan et al., 2009). During Sandy, these data aided in monitoring the large and quickly-evolving wind field.

- 4) Multi-platform tropical cyclone surface wind analysis product  
To overcome some of the issues associated with combining and the interpretation of multiple satellite-based surface and near-surface wind information in the hurricane environment, NOAA's National Environmental Satellite, Data, and Information Service (NESDIS) produces the operational Multi-satellite-platform Tropical Cyclone Surface Wind Analysis (MTCSWA), which combines many of the satellite-based surface and near-surface wind fields for all active global TCs (Knaff et al., 2011). Inputs include previously described AMSU non-linear balance winds, Atmospheric Motion Vectors (AMVs), and ocean surface vector winds from scatterometry, along with infrared based flight-level proxy winds described in Mueller et al. (2006). The analysis system produces wind estimates with generally smaller errors than the raw input data. Although these products were not routinely used by NHC forecasters during Sandy, the product provides an objective blend of multiple satellite wind estimates, which has the potential to assist with wind structure analysis. An example of this product and the four inputs produced on 29 October at 1800 UTC is shown in Fig. 4 when Sandy was off the coast of Delaware and its large wind field was beginning to be felt along the mid-Atlantic coast.

- 5) Objective storm type classification algorithm  
As described above, Sandy was an especially challenging case because of the complex interactions with mid-latitude systems and ET right before landfall in a heavily populated region of the U.S. Forecasters use a variety of sources to make their subjective determination of the storm type. These include global and regional models, and variables diagnosed from the model fields. Hart (2003) showed that thermal wind and circulation asymmetries estimated from global model fields are especially useful in determining whether a cyclone is tropical, subtropical, or extra-tropical. These parameters are used in three-axis phase space diagrams that are available in real time from <http://moe.met.fsu.edu/cyclonephase/> and often utilized by NHC forecasters. The only input required for these diagrams is the geopotential height field. To provide a purely observation based version of these diagrams, a version is

provided that uses the geopotential height analyses from the operational AMSU wind product previously described.

Objective guidance for estimating the storm type is also proved by a classification algorithm added to the operational Statistical Hurricane Intensity Prediction Scheme (SHIPS) model in 2011. The product uses a linear discriminant technique to classify a cyclone as tropical, subtropical or extra-tropical. The input to the algorithm includes parameters from the GFS that are similar to those in the Hart (2003) phase space diagrams, ocean input, and inner core convective features from GOES data. This algorithm worked very well during Hurricane Sandy and correctly predicted the ET.

### 3.2. Track forecasts

Once the initial position and motion of the cyclone are estimated, the track forecasts are determined by a suite of forecast models. A wide variety of satellite data are assimilated to help determine the global model initial conditions. The satellite data are assimilated in two ways. The satellite radiances are included using variational data assimilation systems. In these assimilation systems, the model meteorological fields such as temperature and moisture are used as input to "forward" models that convert them to a form that is equivalent to satellite radiances. The meteorological model fields are then adjusted to minimize the difference between the observed radiances and model-derived radiances. Trace gases such as ozone are also assimilated in this matter. Data from microwave (e.g. AMSU) and infrared (e.g. CrIS) sounders from LEO and Geostationary Operational Environmental Satellites (GOES), respectively, from the U.S. and the international community are critical for accurate track forecasts. For example, McNally (2012) showed that the ECMWF model forecast for Sandy initialized five days prior to the observed landfall was degraded when polar and geostationary satellite data were excluded, with the impact of the LEO data larger than that of the geostationary data. In fact, when the LEO data were excluded, the forecast completely missed the landfall in the U.S.

The second method for including satellite data in models is to assimilate derived products. The most common examples of these are Atmospheric Motion Vectors (AMVs) and retrievals of temperature and humidity. Geostationary satellites are used over most of the globe (Bresky et al., 2012), although, in polar regions, LEO satellite coverage is frequent enough to estimate AMVs as well (Key et al., 2010). By improving the initialization of the environmental wind field, model

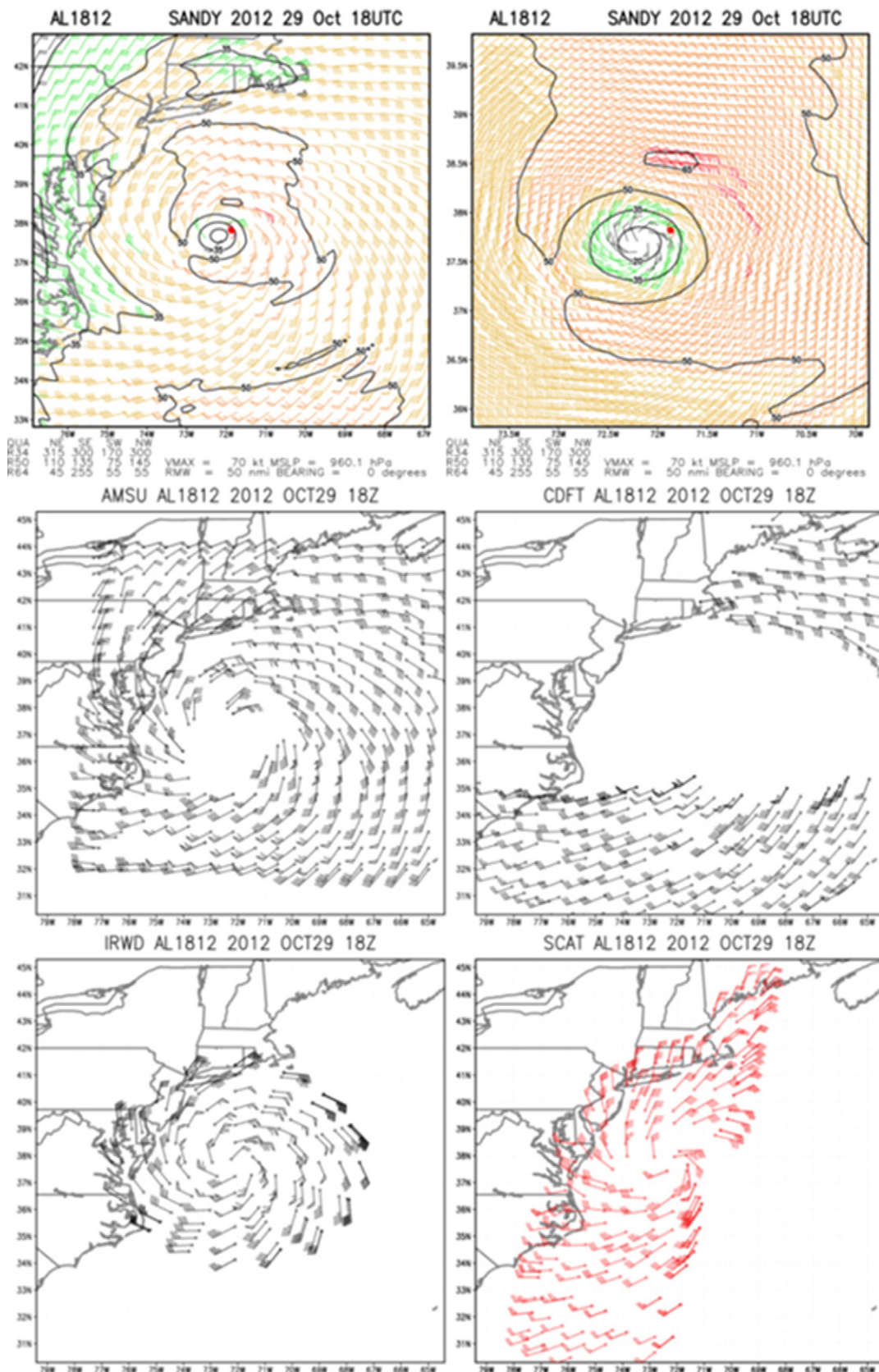


**Fig. 4.** Examples of operational MTCSPA products generated for Hurricane Sandy on 29 October 18 UTC. Note these products have non-SI units that are used in operations. The wind analysis is created at two different scales as shown in the top two panels. The bottom panels show the basic input datasets, namely the AMSU non-linear balanced winds (AMSU), the near-surface atmospheric motion vectors (CDFT), the IR flight-level proxy winds (IRWD), and A-SCAT surface wind vectors (SCAT).

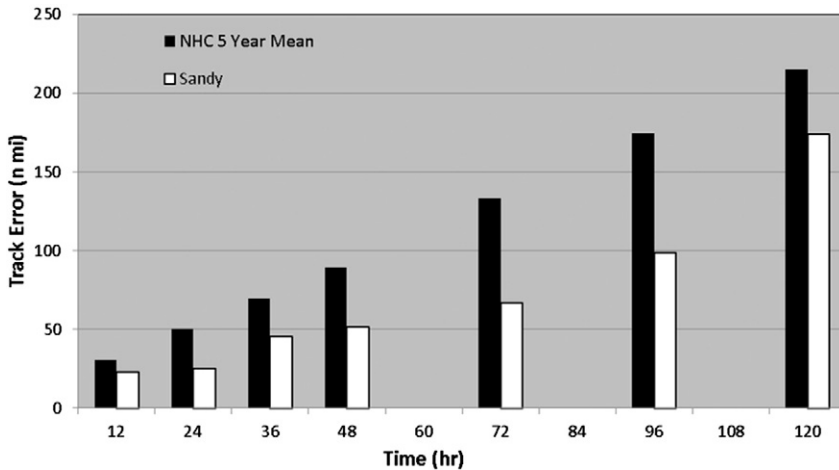


**Fig. 5.** The average track errors of the NHC official forecasts for Sandy compared to the average NHC track errors for the previous five years. Data from Blake et al., 2013.

forecasts of the storm motion and recurvature can be positively impacted (Soden et al., 2001; Goerss et al., 1998; Wu et al., 2014).

The NHC uses several operational global models to forecast TC tracks. These include the GFS and the global models from the ECMWF and the United Kingdom Meteorological Office. Two regional coupled ocean-atmospheric prediction systems, the Geophysical Fluid Dynamics Laboratory (GFDL) hurricane model, and the Hurricane Weather Research and Forecast (HWRF) model, are also used for track forecasting. Regional models are just beginning to directly assimilate satellite data, although these data already impact the regional model forecasts indirectly through the use of the global model fields in the initial and lateral boundary conditions.

Because of its proximity to the U.S. east coast, Sandy was extremely well sampled through the use of satellite data, aircraft reconnaissance data in the storm and in the surrounding near-storm environment, as well as supplemental rawinsondes that were launched over the U.S. for the several days before landfall along the New Jersey coast. These data allowed the operational model forecasts to correctly capture the strong westward curvature of Sandy, which contributed to the NHC track forecast errors for Sandy being much smaller than the previous 5-year average (Fig. 5).

### 3.3. Intensity forecasts

Because of the complexity of the processes involved in TC intensity changes, a hierarchy of intensity forecast models is utilized by the NHC. These models range in complexity from coupled ocean-atmosphere models such as the HWRF model to much simpler statistical-dynamical models such as the Logistic Growth Equation Model (LGEM, DeMaria, 2009) and the SHIPS model, which use statistical post-processing techniques to make intensity forecasts (DeMaria et al., 2014). Similar to the track errors, the NHC official intensity errors for Sandy were 25 to 50% smaller than those from the past 5 years. The primary reason for the low intensity errors was that, except for the initial period of rapid intensification (RI) south of Cuba, the intensity of Sandy changed fairly slowly during much of the storm's lifecycle, making the intensity forecasts somewhat less challenging than usual. The satellite data also contributed to these lower errors through their direct use in the global models, which helped to improve the regional models and the simpler statistical dynamical models, which use input from the global models. As described above for track forecasting, the satellite data improved the forecasts by providing a better representation of the synoptic and near-storm environment. Satellite microwave and infrared radiances, and altimetry are

also used in the analysis of the sea surface temperature and subsurface ocean structure.

Satellite data also contribute in a more direct way to the SHIPS and LGEM models, which include predictors from the GOES imagery and ocean heat content estimates from satellite altimetry. Forecasting rapid intensity change (often defined as an increase in the maximum wind of 30-kt or greater in 24 h) is an especially challenging problem, and neither the dynamical nor statistical models have shown much skill for these cases. For this reason, a specialized statistical model called the rapid intensification index (RII) has been developed, which estimates the probability of RI using model and satellite input (Kaplan et al., 2010). Satellite data input has a much larger influence on the RII than the other statistical techniques. Fig. 6 shows the observed intensity of Sandy and the probability of RI predicted by the RII. Sandy underwent RI from 1800 UTC 23 October until the storm made landfall in western Cuba early on 25 October. The RII predicted probabilities of RI of up to 50% during this period, which is 10 times higher than climatological mean for the Atlantic basin. These very high probabilities were due to the warm sea surface temperatures and large ocean heat content in the Caribbean in an atmospheric environment of low shear. The GOES data indicated that Sandy was very convectively active at this time (not shown), further increasing the probability of RI. Once Sandy

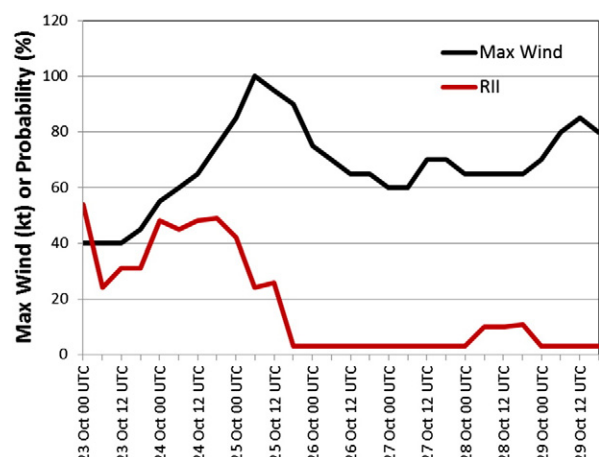


**Fig. 6.** The maximum wind and probability of rapid intensification predicted by the RII for Hurricane Sandy from 23 to 29 October.

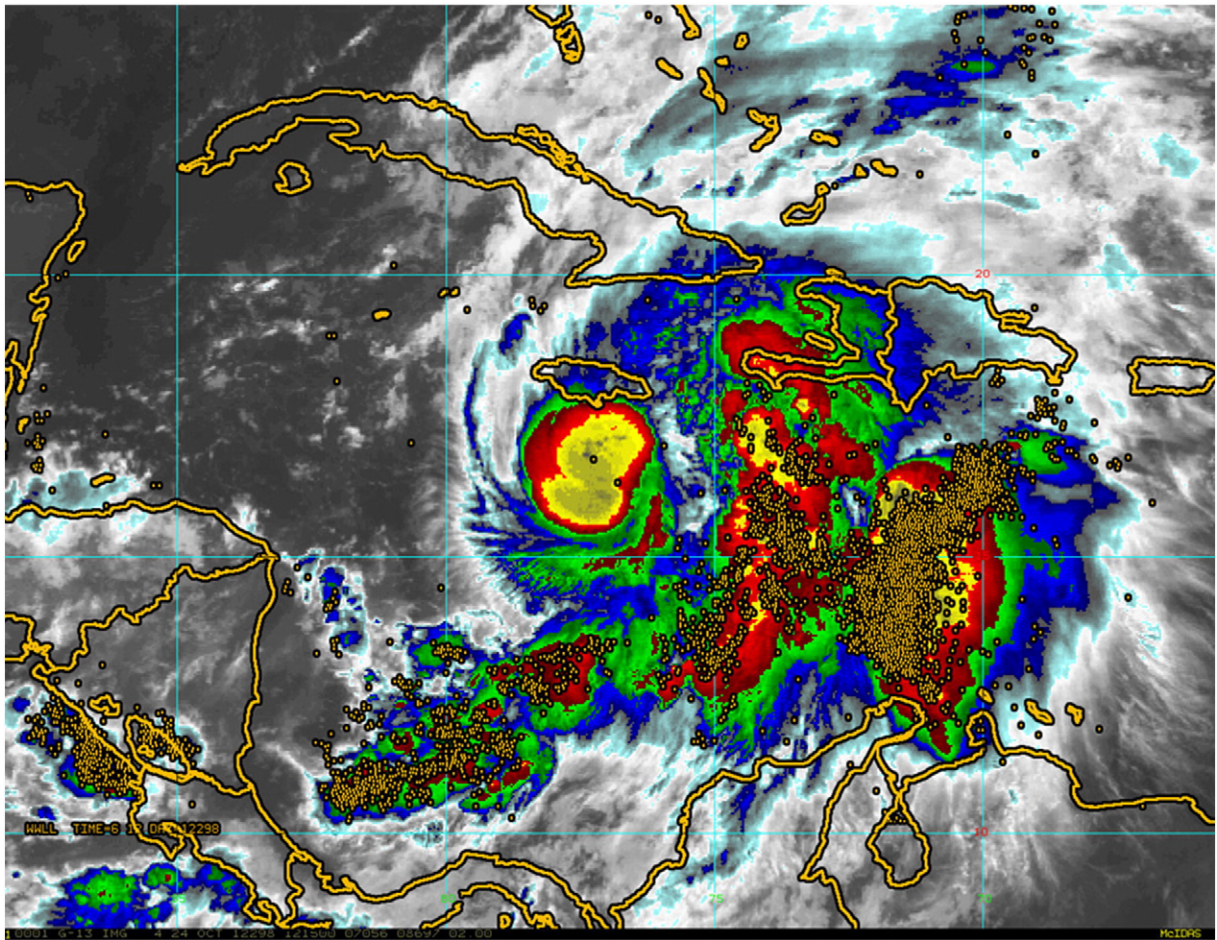


**Fig. 7.** Lightning locations (gold points) within 6 h of 12 UTC on 24 Oct 2012 on a color enhanced GOES IR image.

moved north of Cuba, the oceanic and atmospheric environments were much more hostile for intensification, and the probability of RI remained very low for the rest of Sandy's life cycle. There was a brief period of re-intensification early on 29 October, but it did not satisfy the criterion for RI. Thus, the satellite data input to the RII provided very valuable information for helping to forecast the intensity changes of Sandy.

To prepare for the next generation of geostationary satellites, beginning with GOES-R, an experimental version of the RII with lighting input from a ground-based network has been run as part of the Proving Ground since 2010. DeMaria et al. (2012) showed that enhanced lightning in the rainband region (100–200 km from the center) of TCs is a predictor of RI, and that enhanced lighting in the eyewall region indicates that the RI is near its end. Fig. 7 shows the lightning locations over a 6-h period from the World Wide Lightning Location Network (WWLLN) during the time when Sandy was beginning its RI phase. There was considerable lightning activity away from the storm center, especially to the east of the storm, but very little at the storm center, consistent with the relationship described by DeMaria et al. (2012).

### 3.4. Wind structure prediction

The NHC official forecast includes several parameters that describe the storm structure. The size of the surface wind field is represented by the radius of the maximum extent of 34, 50 and 64-kt winds to the NE, SE, SW and NW of the storm center. Forecasts of the 34 and 50-kt wind radii are provided out to 72 h and 64-kt wind radii forecasts are provided to 36 h. The radii values represent the maximum extent of

those thresholds in each quadrant and are reported in units of n mi (1 n mi = 1.85 km). Estimates and forecasts of the wind structure are important as the relative size of a TC wind field has direct implications for the potential damages (Powell and Reinhold, 2007; Maclay et al., 2008). In addition, the potential for coastal inundation increases with the size of the wind field (e.g., Irish et al., 2008; Lin et al., 2013). The onset of gale (34-kt) and hurricane force (64-kt) winds also occurs earlier in larger TCs, which can hamper pre-storm mitigation efforts.

The primary use of satellite data for wind structure is for the analysis of the wind field described above in Section 3.1. The satellite data were especially useful for Sandy because the wind field extended well beyond the flight legs of the aircraft reconnaissance and the limited availability of buoy data. At the present time, NHC does not have reliable methods for predicting structure changes, other than the use of model forecasts to anticipate extra-tropical transition. As described above for track and intensity forecasting, the satellite data are very important for model initialization, and the global models provided useful guidance on the transition of Sandy just before its final landfall.

### 3.5. Precipitation estimates and forecasts

Satellite derived moisture and precipitation fields serve as complementary sources of information to weather forecasters because they provide information over oceanic regions where in-situ information is limited. This section provides a description of several NESDIS derived products that forecasters use to understand the precipitation field associated with a TC.

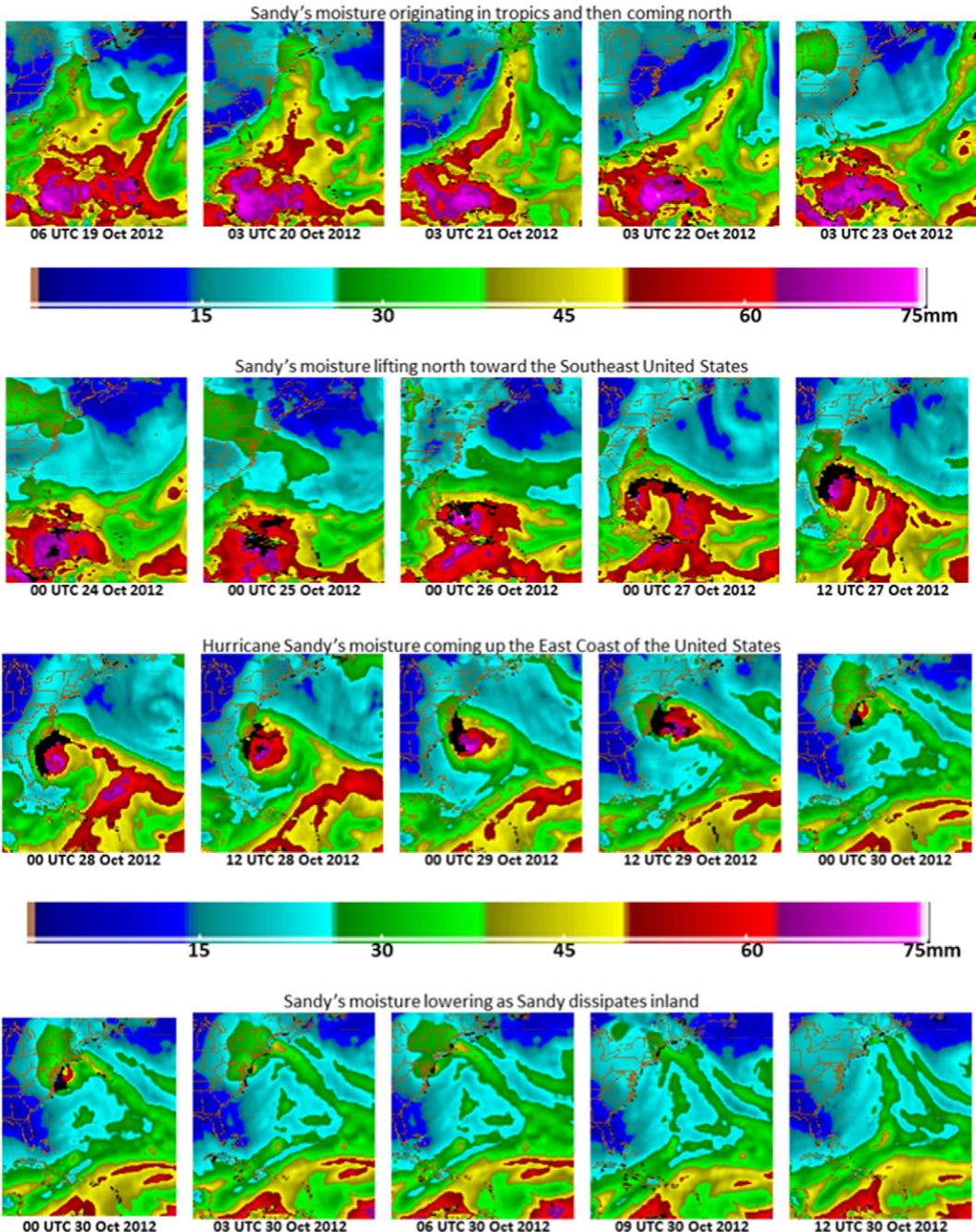


**Fig. 8.** Time sequence of the bTPW product during the life span of Sandy starting at 0600 UTC 19 October 2012 through 1200 UTC 30 October 2012. Units are in mm.

### 3.5.1. Blended Total Precipitable Water (bTPW)

Total Precipitable Water (TPW) is perhaps the most widely used passive microwave product to support real-time forecasting applications, as it accurately depicts tropospheric water vapor and its movement. Early uses of TPW were developed with the Special Sensor Microwave/Imager (SSM/I) (Kusselson, 1993), however, the method has been expanded to include data from all passive microwave sensors, including AMSU. Recently, a multi-sensor approach has been developed and implemented at NESDIS in which passive microwave estimates from multiple satellites and sensors are merged to create a seamless TPW product that is more efficient for forecasters to use (see <http://www.osdpd.noaa.gov/bTPW/>). Additionally, ground-based estimates over land that are derived from the Global Positioning System (GPS)

are also included to anchor the satellite estimates, especially for product continuity across coastlines (Gutman et al., 2004). Most recently, overland estimates are also provided by the Microwave Integrated Retrieval System (MIRS; Boukabara et al., 2011). Details on the blended TPW (bTPW) can be found in Kidder and Jones (2007).

The time sequence of the bTPW product for Sandy is presented in Fig. 8. Here, TPW derived from NOAA-15, NOAA-16, NOAA-18, NOAA-19, MetOp-A and GPS were used to generate the bTPW product. Satellite meteorologists at NESDIS' Satellite Analysis Branch (SAB) provide a national satellite precipitation analysis and short term trend message (the Satellite Precipitation Estimates (SPENES)) in conjunction with the Weather Prediction Center (WPC) forecast rainfall guidance. This information is collectively used by the local National Weather Service

(NWS) Weather Forecast Offices (WFOs), to help issue flood watches and warnings to the public. NESDIS/SAB began to examine the bTPW (and a companion percent of normal product – not shown) to examine the rainfall potential from the system as it began its northward track from the Caribbean Sea toward the U.S. east coast. Interestingly, several days prior to Sandy's landfall, atmospheric moisture streaming north from the system interacted with a frontal system that moved offshore. After a brief drying period, extremely moist air associated with Sandy slowly worked north. Note the extremely high values near the storm's core. Also, in regions of extreme rainfall, the retrieval algorithm becomes unreliable and thus the missing TPW values that are displayed as black pixels. As Sandy made landfall, very moist conditions persisted for several days and contributed to rainfall in excess of 200 mm in the mid-Atlantic. As Sandy became absorbed into the mid-latitude cyclone, the atmospheric moisture slowly decreased.

### 3.5.2. Hydroestimator (H-E)

Until the late 1990s, operational Satellite Precipitation Estimates from NESDIS were produced manually by a NESDIS/SAB satellite analyst using the Interactive Flash Flood Analyzer (IFFA) workstation. Because

of time constraints, estimates could only be produced for a limited number of relatively small regions at a time. In response, NESDIS scientists developed the Auto-Estimator (A-E), which automated many IFFA functions and allowed real-time production of Satellite Precipitation Estimates over the entire continental U.S. (CONUS) with a much shorter lead time than was possible with manually-produced estimates (Scofield and Kuligowski, 2003). The second generation of the A-E is the current Hydro-Estimator (H-E), which improves upon the A-E by distinguishing non-raining cirrus clouds from convectively active, precipitating clouds. All of these products have been the cornerstone of operational satellite precipitation estimation by NESDIS/SAB for the past three decades.

As was described in the previous section, NESDIS/SAB and WPC generated national precipitation nowcasts and forecasts, respectively, which were utilized by the NWS WFOs. As Sandy approached the U.S. mainland, satellite rainfall estimates for various interval periods were available to forecasters (<http://www.star.nesdis.noaa.gov/smcd/emb/ff/>). Also available to forecasters to help them issue flood warnings were 11 SPENES issued by NESDIS/SAB as Sandy approached the Mid-Atlantic region coast and went inland. Fig. 9 shows both the 24-h and

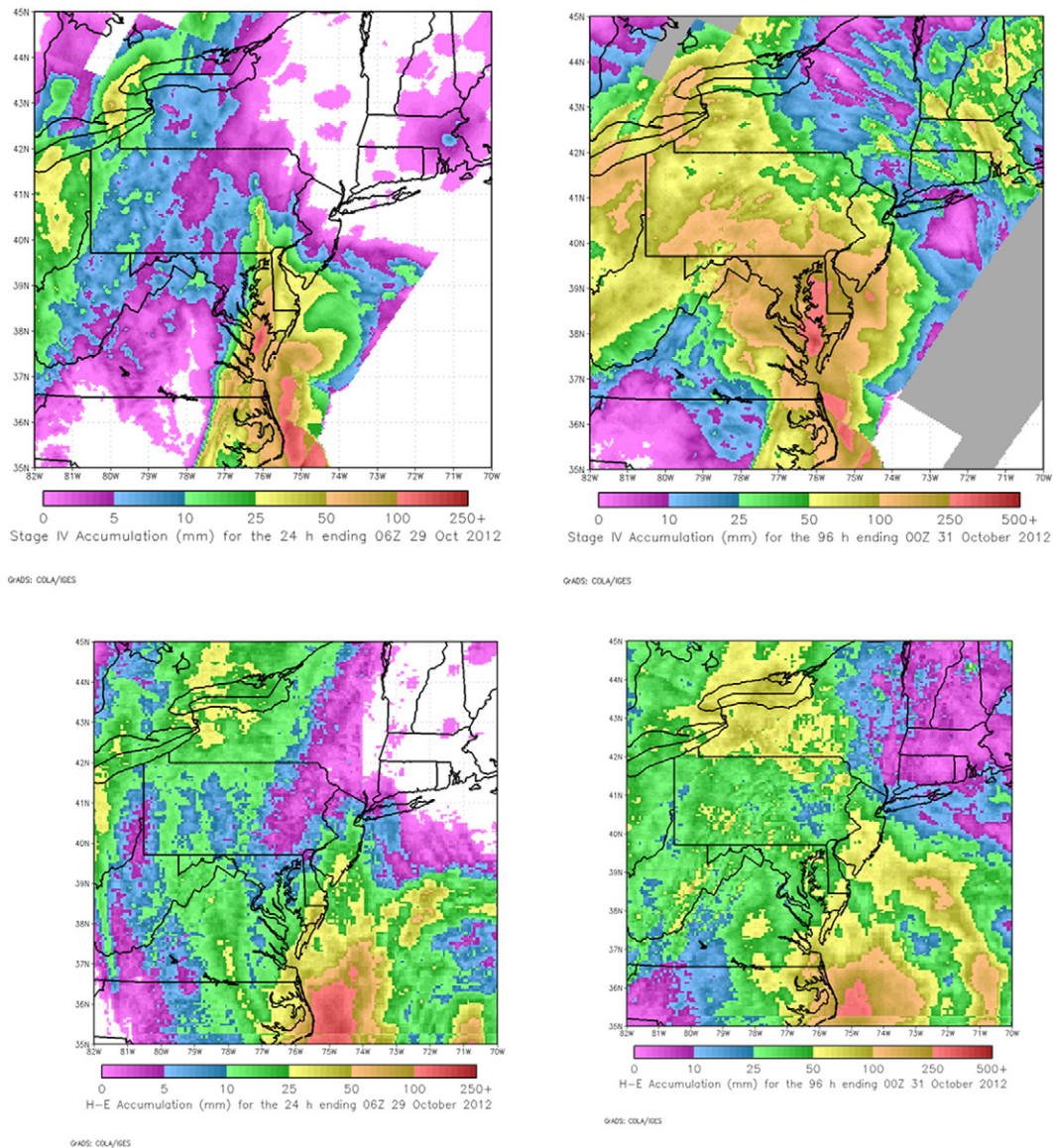


**Fig. 9.** Stage IV 24 h accumulated rainfall (top) through 0600 UTC on 29 October 2012 (left) and 96 h accumulated rainfall through 0000 UTC on 31 October 2012 (right) compared to the Hydroestimator (bottom) for the same time periods (left - 24 h) and right (96 h).

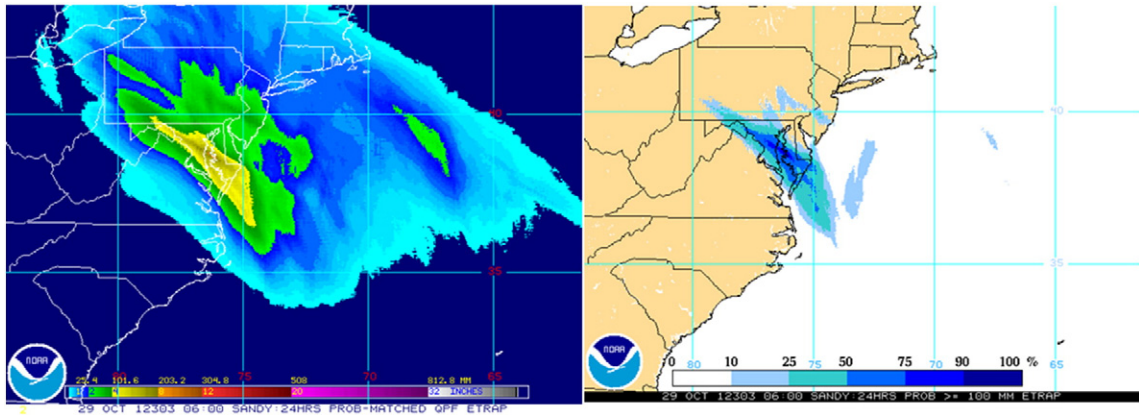


**Fig. 10.** Ensemble TRaP (eTRaP) 24-h rainfall estimates from 0600 UTC 29 October 2012 to 0600 UTC 30 October 2012 (left) and the probability of 100 mm or greater rainfall (right) for the same period.

96-h totals for the H-E and Stage IV (a rain gauge corrected, near-real time radar product generated by the NWS over the CONUS) ending at 0600 UTC on 29 October 2012 and 0000 UTC on 31 October 2012, respectively. As can be seen, the H-E did a reasonable job with the tropical parts of Sandy (i.e. in NC), but underestimated the rainfall in the areas of tropical transition in the Mid-Atlantic States when the cloud tops warmed and the H-E performance weakens. Future techniques under development which fuse satellite microwave estimates with the rapid update GOES visible and infrared (IR) estimates have shown promise to improve the rainfall estimates (Kuligowski et al., 2013).

### 3.5.3. Ensemble Tropical Rainfall Potential (eTRaP)

Heavy rains associated with land falling TCs frequently trigger floods that cause millions of dollars of damage and lost lives. To provide observation-based forecast guidance for TC heavy rain, Kidder et al. (2005) developed the Tropical Rainfall Potential (TRaP), an extrapolation forecast generated by accumulating rainfall estimates from microwave sensors over a 24 hour period as the storm is translated along the forecast track (Kidder et al., 2005). TRaP aims to predict the maximum rainfall at landfall, as well as the spatial pattern of precipitation, and has been shown to have a similar or better skill than short-range numerical weather prediction models (Ferraro et al., 2005; Ebert et al., 2005).

A recent innovation has been to combine the TRaP forecasts from multiple sensors and various start times into an ensemble TRaP product known as eTRaP (Ebert et al., 2011). The ensemble approach provides more accurate quantitative precipitation forecasts, including more

skillful maximum rainfall amount and location, and probabilistic forecasts of rainfall exceeding various thresholds that decision makers can use to make critical risk assessments. Ebert et al. (2011) showed that eTRaP probabilistic forecasts have useful skill, but the grid-scale probabilities are biased high when compared to observations and should be interpreted in a broader spatial context. Efforts to calibrate the probabilistic forecasts from eTRaP are underway.

Shown in Fig. 10 is the 24-hour eTRaP estimate ending 0600 UTC on 29 October 2012 as well as the probability of rainfall exceeding 100 mm. The maximum estimate was approximately 200 mm; the region of predicted rainfall exceeding 100 mm matches very well with the Stage IV estimate (see Fig. 9) on the Delmarva coast, but appears to have overestimated the rainfall further inland where the characteristics of the rain were more stratiform in nature.

### 3.5.4. Microwave snowfall rates

After several years of operating in an experimental mode, a new passive microwave snowfall rate (SFR) algorithm was implemented into NESDIS operations in the fall of 2012 (Meng et al., 2012). Although the product is best suited for use in sparse surface data and radar coverage regions, it is interesting to evaluate its utility and performance during Sandy because of the diverse nature of the storm and the excessive snowfall that was experienced in the higher altitudes of the mid-Atlantic region.

Currently, the AMSU SFR is retrieved using data from four satellites: NOAA-18, -19, Metop-A, and Metop-B. Fig. 11 shows the NOAA-18 SFR at 1924 UTC on 29 October and the coincident next-generation radar

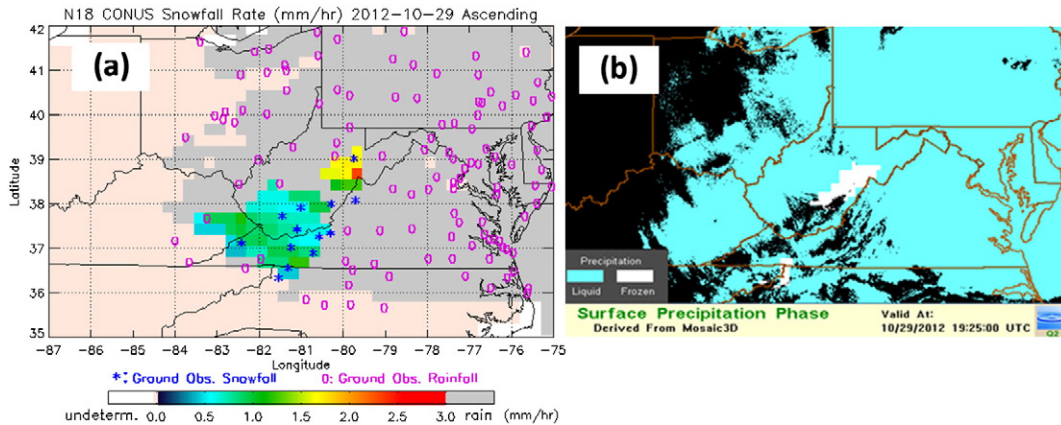


**Fig. 11.** Comparison of the NOAA-18 snowfall rate product, in water equivalent  $\text{mm h}^{-1}$  (a) with the NEXRAD-based National Mosaic and Multi-Sensor QPE (NMO) precipitation phase product (b) on 29 October 2012 at 1925 UTC. Ground observed precipitation type (snowfall — \* and rainfall — o) are also included in (a); gray regions are areas of rain detected by NOAA-18.

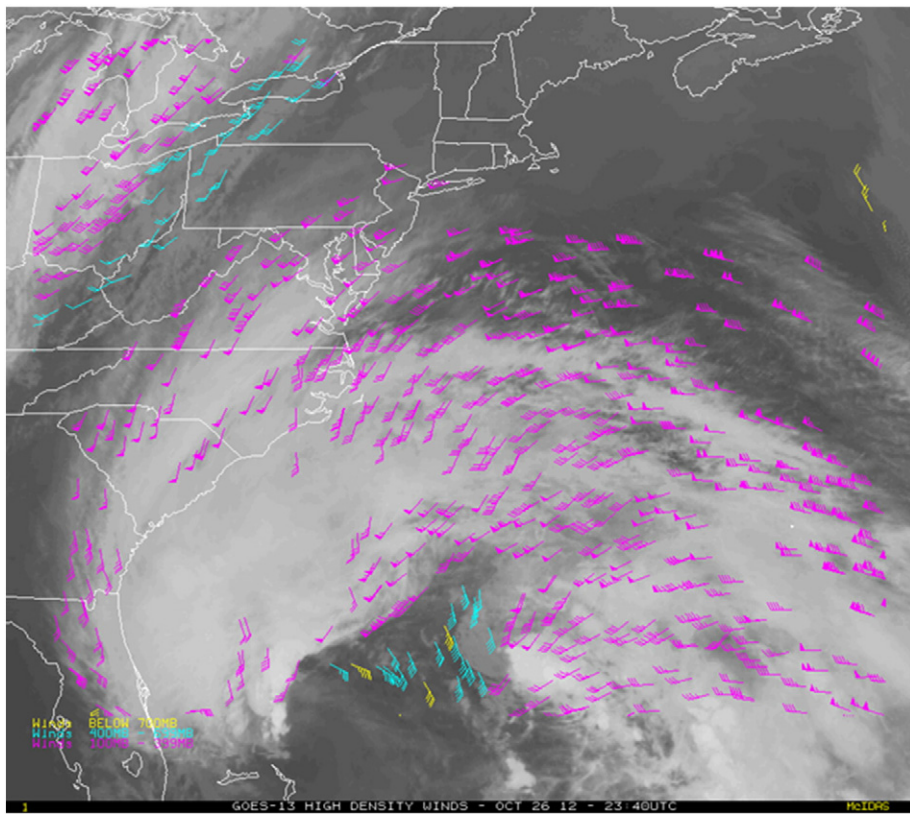


**Fig. 12.** Cloud-drift winds derived from 15-minute GOES-13 11  $\mu\text{m}$  imagery over Hurricane Sandy over the period 27 October (0140 UTC) through 30 October (1240 UTC), 2012. Upper level winds (above 400 hPa) are shown in magenta, mid-level (400–699 hPa) winds are shown in cyan, and lower level (below 700 hPa) are shown in yellow.

(NEXRAD) based National Mosaic and Multi-Sensor Quantitative Precipitation Estimate (NMQ) precipitation phase product. The gray color in the SFR image represents the AMSU retrieved rain area. The SFR image also includes the ground observed precipitation type (snowfall and rainfall). Comparisons with hourly snowfall accumulations measured at weather stations showed reasonable agreement in the overall retrieved snowfall rates. The SFR product had some false alarms along the periphery (i.e. the rain and snow transition zone) compared to ground truth. However, it generally performed better than the NMQ phase product in snowfall detection especially in the mountainous regions in southeastern West Virginia and southwestern Virginia.

#### 4. Emerging satellite and data products

Forecaster at various NWS Weather Forecast Offices and NCEP national centers have been introduced to new satellite products and techniques through Satellite Proving Ground activities which encompass both the Geostationary Operational Environmental Satellite – R-Series (GOES-R) and Joint Polar Satellite System (JPSS) programs. Many of the products utilize the current satellite capabilities from the legacy geostationary and polar-orbiting satellites to create proxy, future capability products for use in operations. During Sandy's evolution and eventual landfall, many of these products were available to forecasters alongside the current imagery and product discussed in the previous section. The GOES-14 Super Rapid Scan Operations for GOES-R (SRSOR) have provided the forecasters with rare, 1-minute imagery that can be used to monitor the near-term intensity and structure changes in a tropical cyclone. With higher temporal resolution offered by the Advanced Baseline Imager (ABI) on GOES-R, Atmospheric Motion Vectors will be more plentiful and will lead to much better model initialization of position and synoptic environment around the tropical

cyclone. New lightning detection algorithms are currently helping to simulate the Geostationary Lightning Mapper (GLM) by providing a more quantitative picture of lightning activity as it relates to rapid intensification and storm organization. Finally, the Advanced Technology Microwave Sounder (ATMS) on the Suomi-National Polar-orbiting Partnership (S-NPP) satellite is providing forecasters with follow-on microwave precipitation products that can be used to monitor precipitation trends and distribution in landfalling tropical cyclones. The ATMS data will also be assimilated into hurricane models to provide improvements to track, intensity and structure forecasts. The Proving Ground has provided some valuable experience and evaluations of the products in high stress, high impact situations. Sections 4.1 and 4.2 will focus on future GOES-R and JPSS instruments and their current proxy counterpart products that were demonstrated during Sandy. The future versions of these products will have valuable operational impacts in future high impact weather situations.

##### 4.1. The Geostationary Operational Environmental Satellite – R-Series (GOES-R)

Over the next few years, the NOAA satellite program is going to experience a significant upgrade to the current GOES suite. The GOES-R program is the next generation of geostationary satellites and a key element of the NOAA mission. This new series of satellites will offer improved instrument technologies that will result in improved detection and observation of meteorological phenomena. This will assist the meteorological community to provide more accurate and timely forecasts. GOES-R will feature two state-of-the-art instruments, the ABI and the GLM, which will provide forecasters with higher resolution imagery (spatially and temporally) along with an advanced lightning detection system, respectively. The first satellite in the GOES-R series

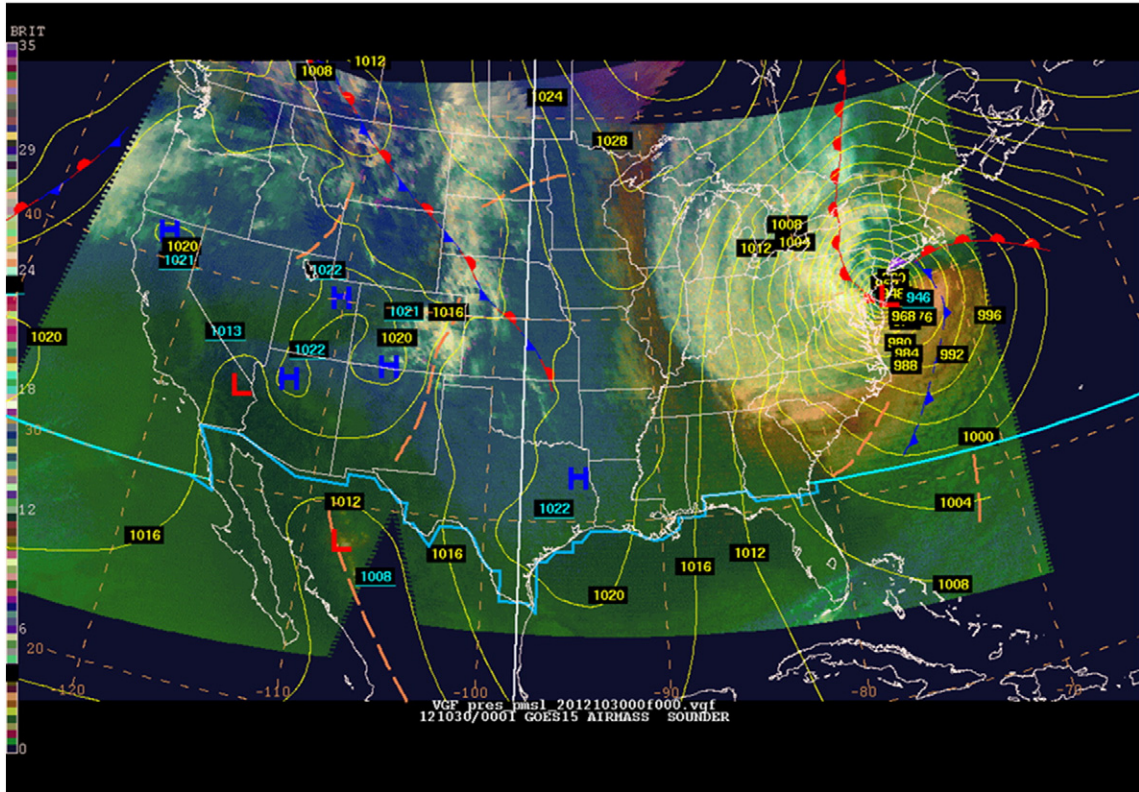


**Fig. 13.** This image shows the interaction of the developing upper-level low near the Carolina coast with Sandy using the RGB Air Mass product overlaid with the WPC 3-hourly surface analyses. Note the drying (orange tint) wrapping around Sandy as the upper-level low and stratospheric intrusion become more dominant.

is scheduled to launch on March 15, 2016, with the first planned operational dates in early 2017.

#### 4.1.1. The Advanced Baseline Imager

The ABI will contain 16 spectral channels at high spatial resolution (0.5 km visible, 1 km near-infrared, 2 km infrared) and high temporal resolution (15 min for full disk, 5 min for CONUS, and 30 s for a meso-scale window or 1-minute if there are two mesoscale regions) (Schmit et al., 2005). The availability of more channels will allow for more multispectral imagery possibilities, similar to those demonstrated in the GOES-R Proving Ground. The GOES-Sounder version of the red, green, blue (RGB) Air Mass product was used during Sandy to analyze the ET using the stratospheric drying as a tracer. Other multispectral combinations will be possible, for example, the RGB Dust (Kerkemann et al., cited, 2013a) or RGB Night-time Microphysics (Kerkemann et al., cited, 2013b) products that are currently being demonstrated using the Spinning Enhanced Visible and Infrared Imager (SEVIRI) on the Meteosat series of satellites or the Moderate Resolution Imaging Spectroradiometer (MODIS) on the National Aeronautics and Space Administration (NASA) Aqua and Terra polar-orbiting satellites. The new spectral bands also allow for a host of quantitative products, such as cloud properties, AMVs, retrievals, SST, dust, and volcanic ash.

**4.1.1.1. Multi-channel imagery products.** Visible, infrared, and water vapor imagery from GOES as well as microwave imagery from LEO satellites were used during Sandy for analysis of the location and initial motion, convective structure and organization, and interactions with synoptic features in the storm environment. The current GOES imager includes five channels, however, GOES-R, will include a 16 channel imager. With this substantial increase in available channels, forecasters will have the ability to use single or multi-channel combinations to

assess the storm environment. Several multi-spectral products are already being utilized by the NHC, as described in more detail below.

As part of the GOES-R Proving Ground activities at NHC, WPC, OPC, and the NESDIS/SAB, the RGB Air Mass product has been introduced to forecasters to monitor TCs and potential ET situations. Multispectral imagery products are available from the GOES-Sounder, the MODIS instrument on NASA's Aqua and Terra satellites, and the combined Visible Infrared Imaging Radiometer Suite (VIIRS) and Cross-track Infrared Sounder (CrIS) on the new Suomi-National Polar-orbiting Partnership (S-NPP) satellite. Details regarding the RGB Air Mass recipe, interpretation table defining the color associated with each air mass, and an additional example application for extratropical cyclogenesis are available in Zavodsky et al. (2013). Forecasters had been introduced to this product in 2011 and found it useful in identifying potential vorticity (PV) anomalies and possible stratospheric intrusions. As the complicated ET of Sandy began to unfold, the RGB Air Mass products provided additional information along with water vapor imagery that was helpful in identifying key ingredients of this transition. The animation in Fig. 13 shows the GOES Sounder version of the RGB Air Mass product which indicates stratospheric drying, designated by the orange coloration in the image, from the deepening eastern U.S. trough interacting and eventually overwhelming the circulation of Sandy. Identification of dry-air entrainment into the storm center helped forecasters define the changeover from a tropical to an extratropical cyclone. More research needs to be done on how this product could assist in future ETs.

**4.1.1.2. Super Rapid Scan Operations for GOES-R.** Another way the unique features of the ABI were demonstrated during Sandy was with continuous Super Rapid Scan Operations for GOES-R (SRSOR) using GOES-14 while it was out of storage for science testing (Schmit et al., 2015). The ABI on GOES-R will be a major improvement on the current GOES imager. For example, the ABI will be operational, in one scan mode it

will provide two center points every minute, have improved spatial resolution, improved bit depth, more spectral bands and improved INR (Image Navigation and Registration). This means that the imagery from the ABI will not have the gaps when a full disk is scanned. These high time resolution image sequences bring the satellite cadence on par with those from other datasets, such as from radar, lightning mapping and other measurements. Not only are the image loops allowing higher time resolution, say to better fix a cyclone location, but also improved products can be derived from the 1-minute data, such as cloud-top cooling or AMVs (Schmit et al., 2013).

**4.1.1.3. Atmospheric Motion Vectors.** Forecasters rely on subjective interpretation of satellite imagery and satellite-derived AMVs to aid in analyzing meteorological conditions over oceanic regions and in the vicinity of TCs (Weldon and Holmes, 1991; Velden et al., 2005). Fig. 12 shows a 3-day loop of GOES-13 infrared window imagery with associated AMVs in the vicinity of Sandy as it moved up the east coast and made landfall in New Jersey.

Satellite AMVs are often the only available wind observations in these situations and provide forecasters with key information on the wind structure, especially with respect to the depiction of upper level wind features and their evolution, which can play a role in TC formation and motion. A continuing challenge to forecasters is the interaction of TCs with upper level troughs, which often affect the storm motion and intensity. Satellite AMVs, which are made available to forecaster display systems, help characterize these interactions during the operational

forecasting process. AMVs are also used in data assimilation to improve analyses and forecasts from numerical weather prediction (NWP) models. With the increased temporal resolution of GOES-R, more AMVs will be available and improved to get a better depiction of the storm environment and synoptic evolution around tropical cyclones.

#### 4.1.2. The Geostationary Lightning Mapper

The GOES-R risk reduction program has increased the use of lightning information in both operational and research environments. Existing lightning detection networks cannot fully replicate the capabilities of the planned GOES-R GLM, but must be used to prepare forecasters for the GLM era (Goodman et al., 2012). The Tropical Rainfall Measuring Mission (TRMM) Lightning Image Sensor (LIS) detects both intra-cloud (IC) and cloud-to-ground (CG) lightning (i.e., total lightning), but only samples while overhead (~90 s snapshots). Ground-based lightning mapping array networks continuously detect total lightning, but only cover small geographical areas (150–200 km radii). Other ground-based networks cover larger areas, but almost exclusively detect CG lightning. Thus, different lightning datasets are used to simulate GLM capabilities depending on the spatial scale and location of the research or operations.

During Sandy, forecasters used observations from the WWLLN (cited 2013) and Global Lightning Dataset 360 (GLD360). These lightning data helped improve storm intensity forecast guidance (see Section 3.3) and visualize individual convective storms within the larger circulation. Although these data provided an important contribution to the intensity

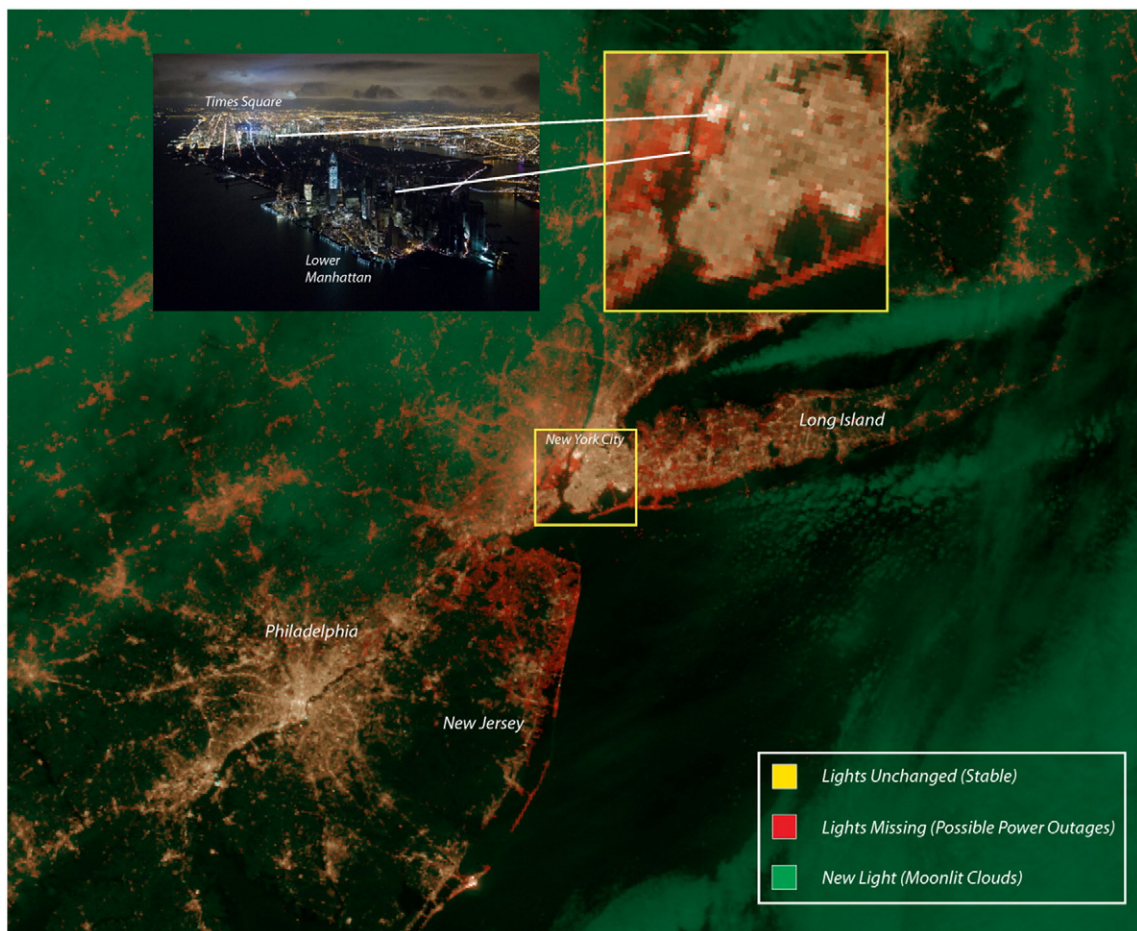


**Fig. 14.** VIIRS Day/Night Band differences imagery between a pre-Sandy ('before') clear sky nighttime scene on 9/26/2013 and a post-Sandy ('after') counterpart on 11/1/2013. In this false color imagery, unchanged (stable) city lights appear as gold, lights that were missing or suppressed in the 'after' image (indicative of either power outages, or cloud obscuration) are red, and brighter lights in the 'after' image (indicative here of moonlit clouds) are green. Red areas devoid of clouds show the widespread extent of coastal outages, with the detail of the zoomed area of Lower Manhattan confirmed by aircraft photography (viewing toward the northeast).

forecast guidance, the existing operational product only plots the locations of individual flashes. These visualizations helped indicate where and when lightning was occurring, but made it difficult to quantify the lightning intensity and how it varied in space and time. This difficulty emphasized the need for a gridded lightning density product to better visualize lightning intensity.

To address this capability, a lightning flash density product was developed for demonstration at the OPC during summer 2013. NESDIS and the OPC developed this product as part of the GOES-R proving ground efforts using data from Vaisala's GLD360 network. The project introduces forecasters to a lightning density product at continental (ocean basin) scales in preparation for the spatial coverage of the planned GLM (8 km resolution to match the GLM resolution), improves the OPC's ability to evaluate offshore convection (structure and intensity), and will gather forecaster feedback to improve the product prior to wider distribution. Although not a perfect GLM proxy (i.e., little to no IC detection), this product can help track convective cells beneath cold cloud shields, distinguish thunderstorms from rain-only areas, identify strengthening or weakening convection, and monitor convective mode and thunderstorm evolution.

#### 4.2. The Joint Polar Satellite System (JPSS)

The JPSS program is the next generation of NOAA's polar orbiting environmental satellites. Through a combined effort between NOAA and the NASA spanning 40 years, the first next-generation satellite launched in October 2011: The NOAA/NASA S-NPP satellite. JPSS represents significant technological and scientific improvements in environmental monitoring and will help advance weather, climate, environmental, and oceanic sciences. JPSS provides operational continuity of the existing NOAA Polar-orbiting Operational Environmental Satellites (POES) along with S-NPP. NOAA is responsible for running and operating the JPSS program, while NASA is responsible for developing and building the JPSS spacecraft. The Suomi-NPP satellite is equipped with some very advanced instruments including the VIIRS, the Advanced Technology Microwave Sounder (ATMS), the CrIS, and the Ozone Mapping and Profiler Suite (OMPS). JPSS-1 is scheduled to launch in 2017.

##### 4.2.1. The Visible Infrared Imager Radiometer Suite (VIIRS)

The VIIRS sensor provides high spatial resolution imagery via 22 narrowband channels (five 375 m imagery "I-Bands," sixteen 750 m moderate "M-Bands," and a 742 m resolution Day-Night Band (DNB)) spanning the optical spectrum (0.4–2 μm). Its 3000 km wide swath ensures complete global coverage (with no gaps between adjacent passes) two times a day with local crossing times of roughly 1330 (daytime, ascending node) and 0130 (nighttime, descending node). Its design draws heritage from NOAA's Advanced Very High-Resolution Radiometer (AVHRR), NASA's MODIS sensors, and the Defense Meteorological Satellite Program (DMSP) Operational Linescan System (OLS). Perhaps the most novel component of VIIRS, building upon the heritage of the OLS, is its DNB—a visible/near-infrared (500–900 nm) sensor which provides the unprecedented ability to measure, via on-board calibration, extremely low levels of light down to  $3e-5 \text{ W m}^{-2} \text{ sr}^{-1}$  (or ~ten million times fainter than incident sunlight). This provides sensitivity to a number of nocturnal light sources (e.g., Lee et al., 2006) and enables the first quantitative use of moonlight (Miller and Turner, 2009).

In terms of TC monitoring, the DNB offers several unique sensing capabilities through all phases of a storm—from initial development, through maturity, and either ET or landfall. These capabilities include the use of moonlight to provide additional detail on low-level circulation, storm top structure, and its ability to detect lightning flash activity in the storm's eye wall and convective rain bands (which may complement WWLLN-based information). A truly unique, and particularly poignant, element of the DNB with regard to land-falling storms is its ability to characterize the post-landfall human impact in terms of mapping power outages. Fig. 14 presents an example of the post-Sandy

devastation, with widespread power outages encoded as red "lights out" pixels via a pairing of co-located before/after images. Such information holds potentially high value to emergency managers and first responders in the distribution of resources/aide in the wake of a land-falling storm—particularly in the scenario of a daytime landfall, leading into the confusion of nighttime triage operations.

##### 4.2.2. The Ozone Mapping and Profiler Suite (OMPS)

In preparation for OMPS, a total column ozone retrieval product has been developed using the NASA Atmospheric Infrared Sounder (AIRS; Aumann et al., 2003), aboard the Aqua satellite. AIRS is a hyperspectral cross-track scanning spectrometer/radiometer with 2378 spectral channels in the infrared and near-infrared that can be used to obtain vertical profiles of ozone for detection of stratospheric air intrusions (SAIs) in and around transitioning cyclones. Anomalously large values of PV in the troposphere are commonly associated with SAIs that are introduced by tropopause folds (Uccellini, 1990) and can be an indicator of a TC undergoing ET. Total column ozone maxima are an appropriate proxy for SAI because descent of ozone-rich stratospheric air requires convergence in the lower stratosphere, which leads to local increases in the total column amount (e.g., Reed, 1950). During Sandy, a near-real time AIRS total column ozone product developed and transitioned by the NASA Short-term Prediction Research and Transition (SPoRT; Jedlovec, 2013) was available to WPC and OPC forecasters in conjunction with the GOES-Sounder RGB Air Mass product to detect the synoptic characteristics of the storm as it underwent ET. Fig. 15 shows an example of the product with PV values from the GFS reanalysis at approximately the time that Sandy was undergoing ET showing the collocation between elevated total ozone values and regions of PV associated with stratospheric air intrusions. Additional details of the product along with another example of its use are highlighted in Zavodsky et al. (2013).

##### 4.2.3. Advanced Technology Microwave Sounder (ATMS)

The ATMS, the next generation of operational microwave sounders, is currently on-board Suomi-NPP and will be part of the future JPSS instrument suite. Like the AMSU, ATMS is a cross-track microwave sounder. It has 22 channels, a wider swath, and higher spatial resolution (~25 km at nadir). Like AMSU, it provides radiances needed for data assimilation and retrieves profiles of atmospheric temperature and moisture for weather forecasting and climate communities. ATMS's higher spatial resolution will improve our ability to resolve the finer horizontal temperature features in the atmosphere. For hurricane applications, ATMS will be better able to resolve the warm core structure. Recently, Yang and Zou (2014) have employed resolution enhancement techniques that have demonstrated improved horizontal storm structure, including those type products described in Section 3. Previous research and techniques, discussed earlier, have shown that the magnitude and depth of the upper-level warming are related to hurricane intensity, while its horizontal scales are related to surface wind structure. Monitoring the vertical temperature structures allows for an independent classification of cyclone type (i.e. cyclone phase space) and assessment of vertical wind shear (Knaff et al., 2004). MIRS retrievals from ATMS became operational in December 2013. Both CIMSS and the Cooperative Institute for Research in the Atmosphere (CIRA) are utilizing ATMS to develop new TC structure assessments and visualization tools for hurricane forecasters.

## 5. Conclusions

Observations from polar-orbiting and geostationary satellites continue to be critical for the monitoring and forecasting of TCs and potential ETs. Radiances and derived products are both assimilated in numerical models and used directly by forecasters. A host of new and improved products is providing even more information on the current state of the TC and its environment. These new products are possible

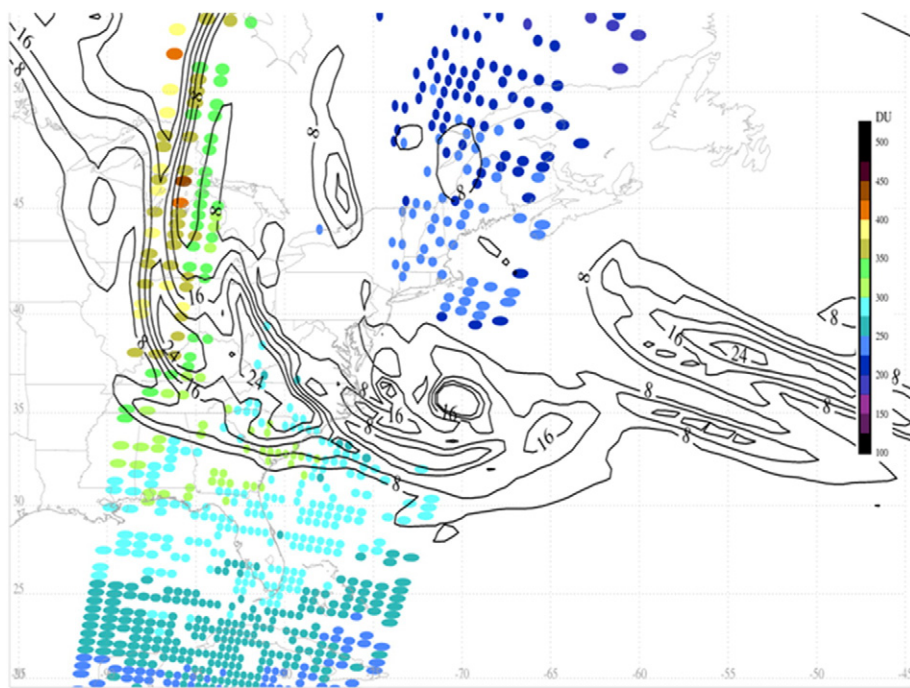


**Fig. 15.** Total column ozone observations (DU) from AIRS at approximately 0700 UTC on 29 October 2012. White areas within the AIRS swath represent profiles that did not pass quality control, which are generally associated with convective clouds. Black contours represent 300 to 500 hPa potential vorticity (PVU; only contours greater than 8 PVU are shown with a contour interval of 4 PVU) from the GFS reanalysis valid at 0600 UTC on 29 October 2012.

due in part to new satellite measurements and in part due to more applied research emerging from NOAA and its academic research partners. These products better monitor the fields of clouds, winds, temperature, moisture/precipitation, aerosols, and the ocean.

As Sandy paralleled and approached the U.S. East Coast, satellite observations provided valuable information on the storm's strength and structure in an otherwise observation-poor region. This allowed forecasters to stress the severity of the situation to emergency managers and government officials to allow for preemptive measures to save as much life and property as possible. Many different satellite products were available to assist with diagnosing the greatest threats ranging from wind and storm surge to an unusual snowstorm for parts of the Appalachians. Future products being demonstrated with existing data in the GOES-R and JPSS Proving Grounds provided forecasters with a sneak peek at the future of satellite technology both during and after Sandy's passage. The quality of the information provided to monitor and help forecast future TC activity will continue to improve over the next decade with the upcoming launches of the GOES-R and JPSS-1 satellites.

## Acknowledgments

The authors would like to acknowledge the contributions from Cezar Kongoli and Banghua Yan. The authors also thank Derrick Herndon, Holly Kessler and Greg DeMaria for data processing and preparing the figures. Finally, the authors would like to thank Julia Pillard for proofing the manuscript. The views, opinions, and findings contained in this report are those of the authors and should not be construed as an official National Oceanic and Atmospheric Administration for U.S. Government position, policy, or decision.

## Appendix A. Supplementary data

Supplementary data to this article can be found online at <http://dx.doi.org/10.1016/j.atmosres.2015.06.005>.

## Appendix B

ABI	Advanced Baseline Imager
AIRS	Atmospheric Infrared Sounder
A-E	Auto-Estimator
AMSU	Advanced Microwave Sounding Unit
AMV	Atmospheric Motion Vector
ASCAT	Advanced Scatterometer
ATMS	Advanced Technology Microwave Sounder
AVHRR	Advanced Very High-Resolution Radiometer
bTPW	Blended Total Precipitable Water
CG	cloud-to-ground (lightning)
CIMSS	Cooperative Institute for Meteorological Satellite Studies
CIRA	Cooperative Institute for Research in the Atmosphere
CONUS	Continental United States
CrIS	Cross-track Infrared Sounder
DMSP	Defense Meteorological Satellite Program
DNB	Day-Night Band
ECMWF	European Centre for Medium-Range Weather Forecast
ET	extratropical transition
eTRaP	Ensemble Tropical Rainfall Potential
GOES	Geostationary Operational Environmental Satellite
GOES-R	Geostationary Operational Environmental Satellite R-series
GFDL	Geophysical Fluid Dynamics Laboratory
GFS	Global Forecast System
GLM	Geostationary Lightning Mapper
GPS	Global Positioning System
H-E	Hydroestimator
HWRF	Hurricane Weather Research and Forecast
IC	intra-cloud (lightning)
IFFA	Interactive Flash Flood Analyzer
INR	Image Navigation and Registration
IR	infrared
JPSS	Joint Polar Satellite System
LEO	low-earth orbiting

LGEM	Logistic Growth Equation Model	Demuth, J.L., DeMaria, M., Knaff, J.A., Vonder Haar, T.H., 2004. Evaluation of Advanced Microwave Sounding Unit tropical-cyclone intensity and size estimation algorithms. <i>J. Appl. Meteorol.</i> 43, 282–296.
LIS	Lightning Image Sensor	Demuth, J.L., DeMaria, M., Knaff, J.A., 2006. Improvement of Advanced Microwave Sounder Unit tropical cyclone intensity and size estimation algorithms. <i>J. Appl. Meteorol.</i> 45, 1573–1581.
MIRS	Microwave Integrated Retrieval System	Ebert, E., Kusselson, S., Turk, M., 2005. Validation of NESDIS operational tropical rainfall potential (TRaP) forecasts for Australian tropical cyclones. <i>Aust. Meteorol. Mag.</i> 54, 121–135.
MODIS	Moderate Resolution Imaging Spectroradiometer	Ebert, E.E., Turk, M., Kusselson, S.J., Yang, J., Seybold, M., Keehn, P.R., Kuligowski, R.J., 2011. Ensemble tropical rainfall potential (eTRaP) forecasts. <i>Weather Forecast.</i> 26, 213–224.
MTCSWA	Multi-satellite-platform Tropical Cyclone Surface Wind Analysis	Ferraro, R., Pellegrino, P., Turk, M., Chen, W., Qiu, S., Kuligowski, R., Kusselson, S., Irving, A., Kidder, S., Knaff, J., 2005. The Tropical Rainfall Potential (TRaP) technique. Part 2: Validation. <i>Weather Forecast.</i> 20, 465–475.
NASA	National Aeronautics and Space Administration	Goerss, J.S., Velden, C.S., Hawkins, J.D., 1998. The impact of multispectral GOES-8 wind information on Atlantic tropical cyclone track forecasts in 1995. Part II: NOGAPS forecasts. <i>Mon. Weather Rev.</i> 126, 1219–1227.
NCEP	National Center for Environmental Prediction	Goodman, S.J., et al., 2012. The GOES-R Proving Ground: Accelerating User Readiness for the Next-Generation Geostationary Environmental Satellite System. <i>Bull. Am. Meteorol. Soc.</i> 93, 1029–1040.
NESDIS	National Environmental Satellite, Data and Information Service	Gutman, S.I., Sahm, S.R., Benjamin, S.G., Schwartz, B.E., Holub, K.L., Stewart, J.Q., Smith, T.L., 2004. Rapid retrieval and assimilation of ground based GPS precipitable water observations at the NOAA Forecast Systems Laboratory: Impact on Weather Forecasts. <i>J. Meteorol. Soc. Jpn.</i> 82, 351–360.
NEXRAD	next-generation radar	Hart, R., 2003. A cyclone phase space derived from thermal wind and thermal asymmetry. <i>Mon. Weather Rev.</i> 131, 585–616.
NHC	National Hurricane Center	Herndon, D., Velden, C.S., 2006. Upgrades to the UW-CIMSS AMSU-based tropical cyclone intensity algorithm. 27th Conference on Hurricanes and Tropical Meteorology, Monterey, CA, pp. 23–28.
NMQ	National Mosaic and Multisensor Quantitative Precipitation Estimation	Irish, J.L., Resio, D.T., Ratcliff, J.J., 2008. The influence of storm size on hurricane surge. <i>J. Phys. Oceanogr.</i> 38, 2003–2013.
NOAA	National Oceanic and Atmospheric Administration	Jedlovec, G., 2013. Transitioning Research Satellite Data to the Operational Weather Community: The SPoRT Paradigm. In: Bruzzone, L. (Ed.), <i>Geoscience and Remote Sensing Newsletter</i> . Institute of Electrical and Electronics Engineers, Inc., New York, pp. 62–66 (March).
NWP	numerical weather prediction	Kaplan, J., DeMaria, M., Knaff, J.A., 2010. A revised tropical cyclone rapid intensification index for the Atlantic and east Pacific basins. <i>Weather Forecast.</i> 25, 220–241.
NWS	National Weather Service	Kerkmann, J., Roesli, H.P., Bridge, G., Konig, M., cited 2013a: Applications of Meteosat Second Generation (MSG), RGB composites with channels 01–11 and their interpretation. [Available on-line at <a href="http://oiswww.eumetsat.org/IPPS/html/bin/guides/msg_rgb_dust.ppt">http://oiswww.eumetsat.org/IPPS/html/bin/guides/msg_rgb_dust.ppt</a> ].
OLS	Operational Linescan System	Kerkmann, J., Roesli, H.P., Bridge, G., Konig, M., cited 2013b: Applications of Meteosat Second Generation (MSG), RGB composites with channels 01–11 and their interpretation. [Available on-line at <a href="http://oiswww.eumetsat.org/IPPS/html/bin/guides/msg_rgb_fog.ppt">http://oiswww.eumetsat.org/IPPS/html/bin/guides/msg_rgb_fog.ppt</a> ].
OMPS	Ozone Mapping and Profiler Suite	Key, J., Santek, D., Dworak, R., Velden, C., Daniels, J., Bailey, A., 2010. The polar wind product suite. <i>Proceedings of the Tenth International Winds Workshop</i> , Tokyo, Japan, February 22–26.
OPC	Ocean Prediction Center	Kidder, S.Q., Jones, A.S., 2007. A blended satellite Total Precipitable Water product for operational forecasting. <i>J. Atmos. Ocean. Technol.</i> 24, 74–81.
OSCAT	Ocean Scatterometer	Kidder, S.Q., Kusselson, S.J., Knaff, J.A., Ferraro, R.R., Kuligowski, R.J., Turk, M., 2005. The Tropical Rainfall Potential (TRaP) technique. Part 1: Description and examples. <i>Weather Forecast.</i> 20, 456–464.
POES	Polar-orbiting Operational Environmental Satellites	Knaff, J.A., Seseske, S.A., DeMaria, M., Demuth, J.L., 2004. On the influences of vertical wind shear on symmetric tropical cyclone structure derived from AMSU. <i>Mon. Weather Rev.</i> 132, 2503–2510.
PV	potential vorticity	Knaff, J.A., DeMaria, M., Molenar, D.A., Sampson, C.R., Seybold, M.G., 2011. An automated, objective, multi-satellite platform tropical cyclone surface wind analysis. <i>J. Appl. Meteorol. Climatol.</i> 50, 2149–2166. <a href="http://dx.doi.org/10.1175/2011JAMC2673.1">http://dx.doi.org/10.1175/2011JAMC2673.1</a> .
RGB	red, green, blue	Kuligowski, R.J., Li, Y., Zhang, Y., 2013. Impact of TRMM data on a low-latency, high-resolution precipitation algorithm for flash flood forecasting. <i>J. Appl. Meteorol. Climatol.</i> 52, 1379–1393.
RI	rapid intensification	Kusselson, S.J., 1993. The operational use of passive microwave data to enhance precipitation forecasts. 13th Conference on Weather Analysis and Forecasting, Vienna, Virginia. <i>Amer. Meteor. Soc.</i> , pp. 434–438.
RII	rapid intensification index	Lee, T.F., et al., 2006. The NPOESS VIIRS Day/Night Visible Sensor. <i>Bull. Am. Meteorol. Soc.</i> 87, 191–199. <a href="http://dx.doi.org/10.1175/BAMS-87-2-191">http://dx.doi.org/10.1175/BAMS-87-2-191</a> .
SAB	Satellite Analysis Branch	Lin, I.-I., Goni, G.J., Knaff, J.A., Forbes, C., Ali, M.M., 2013. Tropical cyclone heat potential for tropical cyclone intensity forecasting and its impact on storm surge. <i>J. Nat. Hazard</i> 66, 1481–1500. <a href="http://dx.doi.org/10.1007/s11069-012-0214-5">http://dx.doi.org/10.1007/s11069-012-0214-5</a> .
SAI	stratospheric air intrusion	Maclay, K.S., DeMaria, M., Vonder Haar, T.H., 2008. Tropical cyclone inner core kinetic energy evolution. <i>Mon. Weather Rev.</i> 136, 4882–4898.
SEVIRI	Spinning Enhanced Visible and Infrared Imager	McNally, T., 2012. Polar data crucial in successful Sandy forecasts. ECMWF Newsletter No. 134, Winter 2012/2013 Available on-line at <a href="http://www.ecmwf.int/publications/newsletters/pdf/134.pdf">http://www.ecmwf.int/publications/newsletters/pdf/134.pdf</a> .
SFR	snowfall rate	Meng, H., Yan, B., Ferraro, R., Kongoli, C., 2012. Snowfall rate retrieval using AMSU/MHS/ATMS measurements. 6th Workshop of the International Precipitation Working Group, São José dos Campos, Brazil, 15–19 October 2012.
SHIPS	Statistical Hurricane Intensity Prediction Scheme	Miller, S.D., Turner, R.E., 2009. A dynamic lunar spectral irradiance dataset for NPOESS/VIIRS Day/Night Band nighttime environmental applications. <i>IEEE Trans. Geosci. Remote Sens.</i> 47 (7), 2316–2329. <a href="http://dx.doi.org/10.1109/TGRS.2009.2012696">http://dx.doi.org/10.1109/TGRS.2009.2012696</a> .
S-NPP	Suomi-National Polar-orbiting Partnership	Mueller, K.J., DeMaria, M., Knaff, J.A., Kossin, J.P., Vonder Haar, T.H., 2006. Objective estimation of tropical cyclone wind structure from infrared satellite data. <i>Weather Forecast.</i> 21, 990–1005.
SPENES	Satellite Precipitation Estimates	
SPoRT	Short-term Prediction Research and Transition	
SRSR	Super Rapid Scan Operations for GOES-R	
SSM/I	Special Sensor Microwave/Imager	
TC	tropical cyclone	
TPW	Total Precipitable Water	
TRaP	Tropical Rainfall Potential	
TRMM	Tropical Rainfall Measuring Mission	
VIIRS	Visible Infrared Imaging Radiometer Suite	
WFO	Weather Forecast Office	
WPC	Weather Prediction Center	
WWLLN	World Wide Lightning Location Network	

## References

- Aumann, H.H., et al., 2003. AIRS/AMSU/HSB on the Aqua Mission: Design, Science Objectives, Data Products, and Processing Systems. *IEEE Trans. Geosci. Remote Sens.* 41, 253–264.
- Bessho, K., DeMaria, M., Knaff, J.A., 2006. Tropical cyclone wind retrievals from the Advanced Microwave Sounder Unit (AMSU): Application to surface wind analysis. *J. Appl. Meteorol.* 45, 399–415.
- Blake, E.S., Kimberlain, T.B., Berg, R.J., Cangialosi, J.P., Beven II, J.L., 2013. Tropical Cyclone Report: Hurricane Sandy. [http://www.nhc.noaa.gov/data/tcr/AL182012\\_Sandy.pdf](http://www.nhc.noaa.gov/data/tcr/AL182012_Sandy.pdf).
- Boukabara, S.-A., Garrett, K., Chen, W., Iturbide-Sánchez, F., Grassotti, C., Kongoli, C., Chen, R., Liu, Q., Yan, B., Weng, F., Ferraro, R., Kleespies, T., Meng, H., 2011. MiRS: An All-Weather IDVARSatellite Data Assimilation & Retrieval System. *IEEE Trans. Geosci. Remote Sens.* 49, 3249–3272.
- Brennan, M.J., Hennon, C.C., Knabb, R.D., 2009. The Operational Use of QuikSCAT Ocean Surface Winds at the National Hurricane Center. *Weather Forecast.* 24, 621–645.
- Bresky, W., Daniels, J., Bailey, A., WanZong, S., 2012. New Methods Towards Minimizing the Slow Speed Bias Associated With Atmospheric Motion Vectors (AMVs). *J. Appl. Meteorol. Climatol.* 51, 2137–2151.
- DeMaria, M., 2009. A simplified dynamical system for tropical cyclone intensity prediction. *Mon. Weather Rev.* 137 (1), 68–82.
- DeMaria, M., DeMaria, R.T., Knaff, J., Molenar, D., 2012. Tropical cyclone lighting and rapid intensity changes. *Mon. Weather Rev.* 140, 1828–1842.
- DeMaria, M., Sampson, C.R., Knaff, J.A., Musgrave, K.D., 2014. Is tropical cyclone intensity guidance improving? *Bull. Amer. Meteor. Soc.* 95, 387–398.
- Demuth, J.L., DeMaria, M., Knaff, J.A., Vonder Haar, T.H., 2004. Evaluation of Advanced Microwave Sounding Unit tropical-cyclone intensity and size estimation algorithms. *J. Appl. Meteorol.* 43, 282–296.
- Demuth, J.L., DeMaria, M., Knaff, J.A., 2006. Improvement of Advanced Microwave Sounder Unit tropical cyclone intensity and size estimation algorithms. *J. Appl. Meteorol.* 45, 1573–1581.
- Ebert, E., Kusselson, S., Turk, M., 2005. Validation of NESDIS operational tropical rainfall potential (TRaP) forecasts for Australian tropical cyclones. *Aust. Meteorol. Mag.* 54, 121–135.
- Ebert, E.E., Turk, M., Kusselson, S.J., Yang, J., Seybold, M., Keehn, P.R., Kuligowski, R.J., 2011. Ensemble tropical rainfall potential (eTRaP) forecasts. *Weather Forecast.* 26, 213–224.
- Ferraro, R., Pellegrino, P., Turk, M., Chen, W., Qiu, S., Kuligowski, R., Kusselson, S., Irving, A., Kidder, S., Knaff, J., 2005. The Tropical Rainfall Potential (TRaP) technique. Part 2: Validation. *Weather Forecast.* 20, 465–475.
- Goerss, J.S., Velden, C.S., Hawkins, J.D., 1998. The impact of multispectral GOES-8 wind information on Atlantic tropical cyclone track forecasts in 1995. Part II: NOGAPS forecasts. *Mon. Weather Rev.* 126, 1219–1227.
- Goodman, S.J., et al., 2012. The GOES-R Proving Ground: Accelerating User Readiness for the Next-Generation Geostationary Environmental Satellite System. *Bull. Am. Meteorol. Soc.* 93, 1029–1040.
- Gutman, S.I., Sahm, S.R., Benjamin, S.G., Schwartz, B.E., Holub, K.L., Stewart, J.Q., Smith, T.L., 2004. Rapid retrieval and assimilation of ground based GPS precipitable water observations at the NOAA Forecast Systems Laboratory: Impact on Weather Forecasts. *J. Meteorol. Soc. Jpn.* 82, 351–360.
- Hart, R., 2003. A cyclone phase space derived from thermal wind and thermal asymmetry. *Mon. Weather Rev.* 131, 585–616.
- Herndon, D., Velden, C.S., 2006. Upgrades to the UW-CIMSS AMSU-based tropical cyclone intensity algorithm. 27th Conference on Hurricanes and Tropical Meteorology, Monterey, CA, pp. 23–28.
- Irish, J.L., Resio, D.T., Ratcliff, J.J., 2008. The influence of storm size on hurricane surge. *J. Phys. Oceanogr.* 38, 2003–2013.
- Jedlovec, G., 2013. Transitioning Research Satellite Data to the Operational Weather Community: The SPoRT Paradigm. In: Bruzzone, L. (Ed.), *Geoscience and Remote Sensing Newsletter*. Institute of Electrical and Electronics Engineers, Inc., New York, pp. 62–66 (March).
- Kaplan, J., DeMaria, M., Knaff, J.A., 2010. A revised tropical cyclone rapid intensification index for the Atlantic and east Pacific basins. *Weather Forecast.* 25, 220–241.
- Kerkmann, J., Roesli, H.P., Bridge, G., Konig, M., cited 2013a: Applications of Meteosat Second Generation (MSG), RGB composites with channels 01–11 and their interpretation. [Available on-line at [http://oiswww.eumetsat.org/IPPS/html/bin/guides/msg\\_rgb\\_dust.ppt](http://oiswww.eumetsat.org/IPPS/html/bin/guides/msg_rgb_dust.ppt)].
- Kerkmann, J., Roesli, H.P., Bridge, G., Konig, M., cited 2013b: Applications of Meteosat Second Generation (MSG), RGB composites with channels 01–11 and their interpretation. [Available on-line at [http://oiswww.eumetsat.org/IPPS/html/bin/guides/msg\\_rgb\\_fog.ppt](http://oiswww.eumetsat.org/IPPS/html/bin/guides/msg_rgb_fog.ppt)].
- Key, J., Santek, D., Dworak, R., Velden, C., Daniels, J., Bailey, A., 2010. The polar wind product suite. *Proceedings of the Tenth International Winds Workshop*, Tokyo, Japan, February 22–26.
- Kidder, S.Q., Jones, A.S., 2007. A blended satellite Total Precipitable Water product for operational forecasting. *J. Atmos. Ocean. Technol.* 24, 74–81.
- Kidder, S.Q., Kusselson, S.J., Knaff, J.A., Ferraro, R.R., Kuligowski, R.J., Turk, M., 2005. The Tropical Rainfall Potential (TRaP) technique. Part 1: Description and examples. *Weather Forecast.* 20, 456–464.
- Knaff, J.A., Seseske, S.A., DeMaria, M., Demuth, J.L., 2004. On the influences of vertical wind shear on symmetric tropical cyclone structure derived from AMSU. *Mon. Weather Rev.* 132, 2503–2510.
- Knaff, J.A., DeMaria, M., Molenar, D.A., Sampson, C.R., Seybold, M.G., 2011. An automated, objective, multi-satellite platform tropical cyclone surface wind analysis. *J. Appl. Meteorol. Climatol.* 50, 2149–2166. <http://dx.doi.org/10.1175/2011JAMC2673.1>.
- Kuligowski, R.J., Li, Y., Zhang, Y., 2013. Impact of TRMM data on a low-latency, high-resolution precipitation algorithm for flash flood forecasting. *J. Appl. Meteorol. Climatol.* 52, 1379–1393.
- Kusselson, S.J., 1993. The operational use of passive microwave data to enhance precipitation forecasts. 13th Conference on Weather Analysis and Forecasting, Vienna, Virginia. *Amer. Meteor. Soc.*, pp. 434–438.
- Lee, T.F., et al., 2006. The NPOESS VIIRS Day/Night Visible Sensor. *Bull. Am. Meteorol. Soc.* 87, 191–199. <http://dx.doi.org/10.1175/BAMS-87-2-191>.
- Lin, I.-I., Goni, G.J., Knaff, J.A., Forbes, C., Ali, M.M., 2013. Tropical cyclone heat potential for tropical cyclone intensity forecasting and its impact on storm surge. *J. Nat. Hazard* 66, 1481–1500. <http://dx.doi.org/10.1007/s11069-012-0214-5>.
- Maclay, K.S., DeMaria, M., Vonder Haar, T.H., 2008. Tropical cyclone inner core kinetic energy evolution. *Mon. Weather Rev.* 136, 4882–4898.
- McNally, T., 2012. Polar data crucial in successful Sandy forecasts. ECMWF Newsletter No. 134, Winter 2012/2013 Available on-line at <http://www.ecmwf.int/publications/newsletters/pdf/134.pdf>.
- Meng, H., Yan, B., Ferraro, R., Kongoli, C., 2012. Snowfall rate retrieval using AMSU/MHS/ATMS measurements. 6th Workshop of the International Precipitation Working Group, São José dos Campos, Brazil, 15–19 October 2012.
- Miller, S.D., Turner, R.E., 2009. A dynamic lunar spectral irradiance dataset for NPOESS/VIIRS Day/Night Band nighttime environmental applications. *IEEE Trans. Geosci. Remote Sens.* 47 (7), 2316–2329. <http://dx.doi.org/10.1109/TGRS.2009.2012696>.
- Mueller, K.J., DeMaria, M., Knaff, J.A., Kossin, J.P., Vonder Haar, T.H., 2006. Objective estimation of tropical cyclone wind structure from infrared satellite data. *Weather Forecast.* 21, 990–1005.

- Powell, M.D., Reinhold, T.A., 2007. Tropical cyclone destructive potential by integrated kinetic energy. *Bull. Am. Meteorol. Soc.* 88, 513–526.
- Reed, R.J., 1950. The Role of Vertical Motions in Ozone–Weather Relationships. *J. Meteorol.* 7, 263–267.
- Schmit, T.J., Gunshor, M.M., Menzel, W.P., Li, J., Bachmeier, S., Gurka, J.J., 2005. Introducing the Next-generation Advanced Baseline Imager (ABI) on GOES-R. *Bull. Am. Meteorol. Soc.* 8, 1079–1096 (August).
- Schmit, T.J., et al., 2013. GOES-14 Super Rapid Scan Operations to Prepare for GOES-R. *J. Appl. Remote Sens.* 7 (1), 073462. <http://dx.doi.org/10.1117/1.JRS.7.073462>.
- Schmit, T.J., et al., 2015. Rapid Refresh Information of Significant Events: Preparing users for the next generation of geostationary operational satellites. *Bull. Am. Meteorol. Soc.* 96, 561–576. <http://dx.doi.org/10.1175/BAMS-D-13-00210.1>.
- Schofield, R.A., Kuligowski, R.J., 2003. Status and outlook of operational satellite precipitation algorithms for extreme-precipitation events. *Mon. Weather Rev.* 131, 1883–1898.
- Soden, B.J., Velden, C.S., Tuleya, R.E., 2001. The impact of satellite winds on experimental GFDL hurricane model forecasts. *Mon. Weather Rev.* 129, 835–852.
- Uccellini, L.W., 1990. Processes contributing to the rapid development of extratropical cyclones. In: Newton, C., Holopainen, E.H. (Eds.), *Extratropical Cyclones: The Erik Palmén Memorial Volume*, pp. 81–105.
- Velden, C., Daniels, J., Stettner, D., Santek, D., Key, J., Dunnion, J., Homlund, K., Dengel, G., Bresky, W., Menzel, W.P., 2005. Recent Innovations in Deriving Tropospheric Winds from Meteorological Satellites. *Bull. Am. Meteorol. Soc.* 86, 205–233.
- Velden, C., Harper, B., Wells, F., Beven II, J.L., Zehr, R., Olander, T., Mayfield, M., Guard, C., Lander, M., Edson, R., Avila, L., Burton, A., Turk, M., Kikuchi, A., Christian, A., Caroff, P., McCrone, P., 2006. The Dvorak tropical cyclone intensity estimation technique. A satellite-based method that has endured for over 30 years. *Bull. Am. Meteorol. Soc.* 87, 1195–1210.
- Weldon, R.B., Holmes, S.J., 1991. Water vapor imagery: Interpretation and applications to weather analysis and forecasting. NOAA Tech Report NESDIS 67 (213 pp.).
- Wu, T.C., Liu, H., Velden, C., Majumdar, S., Anderson, J., 2014. Influence of Assimilating Satellite-Derived Atmospheric Motion Vector Observations on Numerical Analyses and Forecasts of Tropical Cyclone Track and Intensity. *Mon. Weather Rev.* 142, 49–71.
- Yang, H., Zou, X., 2014. Optimal ATMS Remapping Algorithm for Climate Research. *IEEE Trans. Geosci. Remote Sens.* 11, 7290–7296.
- Zavodsky, B.T., Molthan, A.L., Folmer, M.J., 2013. Multispectral Imagery for Detecting Stratospheric Air Intrusions Associated with Mid-Latitude Cyclones. *J. Oper. Meteorol.* 1, 71–83.